Geology Geophysics and Earth Science
Volume 2, Issue 2, No. 2
Received 19 January 2024; Accepted 2 February 2024
Published online 18 February 2024

Sanderman Publishing House

The reasons for enormous accumulation of the geodynamic tension in Eastern Turkey: a multidisciplinary study

Lev Eppelbaum[1,2], Youri Katz[3] and Zvi Ben-Avraham[1]
[1]Department of Geophysics, Faculty of Exact Sciences, Tel Aviv University, Ramat Aviv, Tel Aviv, Israel
[2]Azerbaijan State Oil and Industry University, 20 Azadlig Ave., Baku, Azerbaijan
[3]Steinhardt Museum of Natural History & National Research Center, Faculty of Life Sciences, Tel Aviv University, Ramat Aviv, Tel Aviv, Israel

Abstract. The catastrophic earthquakes in Eastern Turkey (Eastern Mediterranean) require their geodynamic understanding. The two most decisive events with magnitudes of 7.95 and 7.86 on 06.02.2023, followed by a series of more than 10,000 significant aftershocks. These tragic events led to the death of more than 60 thousand people. The above values indicate the colossal tension created in the Earth's crust. The region where these strongest earthquakes occurred is a complex junction zone of four tectonic plates: Eurasian, Arabian, African, and Anatolian. The joint movement of these plates (consisting, in turn, of tectonic elements of different ages) occurs at an average rate of 6–18 mm per year. After two marked powerful shocks and a series of aftershocks, some sectors of the Anatolian plate shifted to the southwest by more than 11 meters. Our recent publications indicated the presence of a giant, rotating quasi-ring structure below the Easternmost Mediterranean. This research contains significant newly obtained data. The quantitative analysis of the satellite-derived gravity data indicates the lower mantle occurrence of the anomalous target. Examination of the geoid anomalies map also testifies to the deep origin of this structure. The regional seismic tomography data confirm the presence of anomalous zones at a depth of 1500-1700 km. The GPS vector map and the comprehensive review of paleomagnetic data display the counterclockwise rotation of this structure. Analysis of the recently constructed magnetic field ΔZ pattern commonly proves the presence of this quasi-ring structure. The newly developed paleobiogeographic map is consistent with the proposed physical–geological model. A widespread analysis of tectonic, petrological, and mineralogical data implies a connection between the discovered deep structure and near-surface processes. A crucial for understanding the nature of the considered seismic stress is its location near the expressed bend of the Mesozoic terrane belt, where the Arabian Plate is deeply intruded into the Alpine-Himalayan belt. Thus, the rotation of this giant deep structure may accumulate the stress effect retrieved from the satellite, airborne, and surface geophysical observations. We propose that this stress, along with the known Earth's crust seismological activity in this region, is the causative reason for the catastrophic geodynamic events in Eastern Turkey.

Keywords. Geodynamics, GPS, gravity, magnetic and paleomagnetic data analysis, geoid isolines, paleobiogeographical scheme, integrated analysis, counterclockwise rotation.

1. Introduction

Studying the interactions between deep geodynamics and surface (subsurface; the last term here can mean many tens of km) geological processes is one of the critical problems in solid earth sciences [1–6]. A series of catastrophic seismic events in southeastern Turkey in February 2023 [7] makes it necessary to consider the diverse tectonic-geodynamic and deep geophysical data to explain this natural phenomenon. This complex analysis procedure is necessary for developing regional monitoring of the sustainability of habitats and engineering infrastructures of this area – one of the most ancient in civilizational development. Non-conventional tectonic-structural features of the mantle, lithosphere, and hydrosphere cause the anomalousness of the region. A complex junction of oceanic and continental crust units is a distinguishing feature of the study region. The simultaneous development of collision processes (associated with the latitudinal zone of the Neotethys Ocean closure) and the manifestation of the initial stages of spreading of the Red Sea–Indian Ocean submeridional rift system further complicates the overall pattern.

The region where these strongest earthquakes occurred is a tectonically complex junction zone of four tectonic plates: Eurasian, Arabian, African, and Anatolian [8–13]. Tectonically, the considered area belongs to the Eastern Mediterranean, with its Cyprus-Levantine marine and Anatolian-Nubian-Arabian continental framing (Figure 1). The joint movement of these plates (consisting, in turn, of tectonic elements of different ages) occurs at an average rate of 6–18 mm per year [14]. However, after two marked powerful shocks on 06.02.2023, the Anatolian plate shifted to the southwest by several meters (two tectonic segments – up to 11.2 and 11.5 m). These tragic events led to more than 60 thousand deaths and destroyed many buildings and engineering constructions. What is the main reason for such a powerful geodynamic event? We suggest that these catastrophic events were triggered by the recently discovered mantle quasi-circular counterclockwise rotating structure [15, 16], influencing many subsurface processes. At the same time, we must note that these events were impossible without combining counterclockwise rotation with the intensive surface (subsurface) seismological activity [e.g., 17, 18] in Eastern Turkey.

Applying one or two geophysical (geological) methods is insufficient to analyze such a complex phenomenon. Besides attracting different geophysical and geological methods, the combination of deterministic and probabilistic approaches [e.g., 19, 20] should be used here.

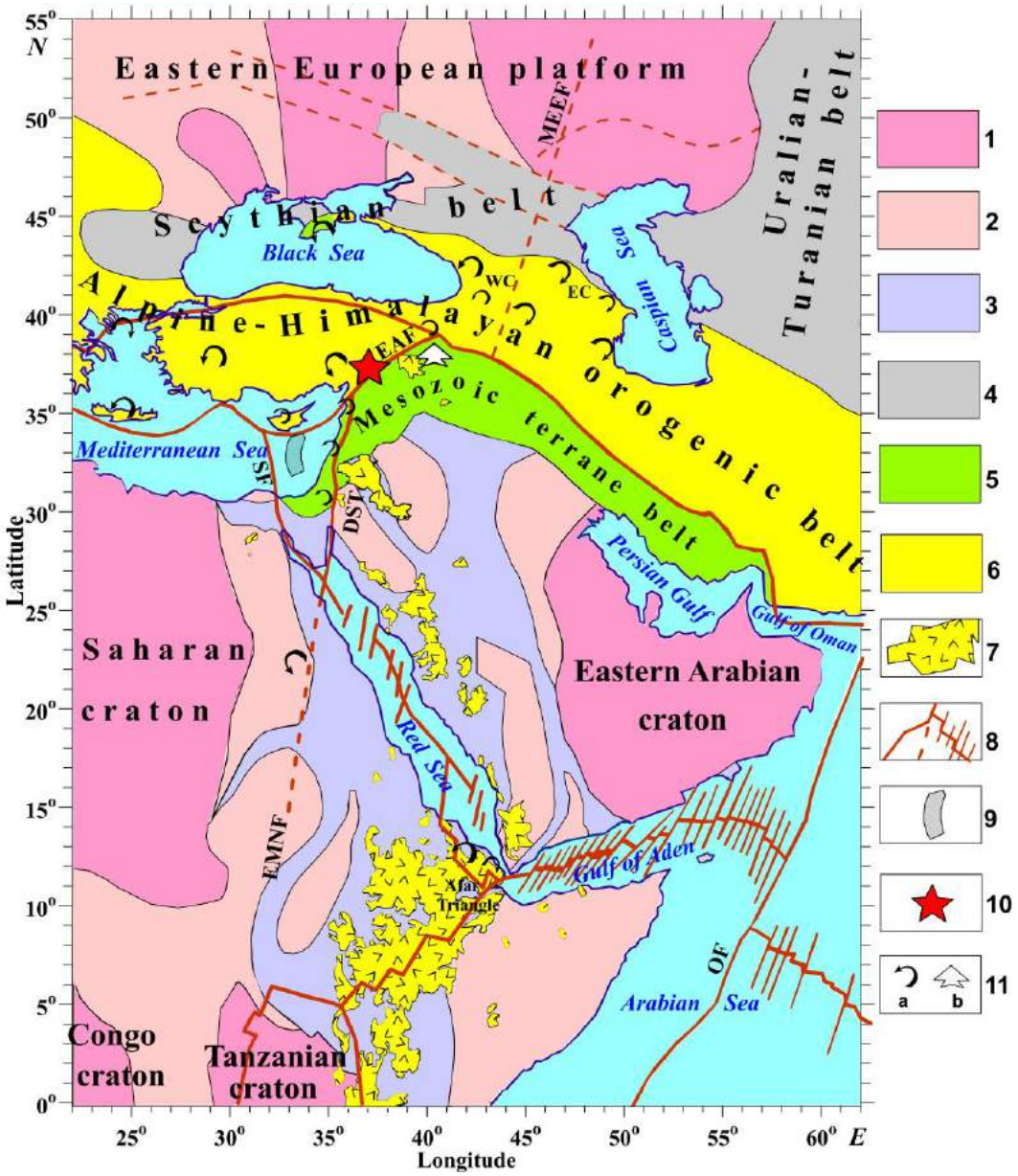

Figure 1. The tectonic-geodynamic scheme of the region under study (modified after [16]). (1) Archean cratons, (2-4) folded belts: (2) Paleo-Middleproterozoic, (3) Neoproterozoic, (4) Late Paleozoic (Herzynian), (5) Mesozoic terrane belt (MTB), (6) Alpine-Himalayan orogenic belt, (7) Cenozoic traps of the African-Arabian rift belt, (8) main fault systems, (9) contour of the Kiama paleomagnetic hyperzone of inverse polarity [21, 22], (10) high magnitude seismogenic zone in Eastern Turkey (February 06, 2023), (11) **a**: rotational geodynamic elements derived from paleomagnetic data, **b**: distal part of the MTB. SF, Sinai Fault, DST, Dead Sea Transform, MEEF, Main Eastern European Fault, EMNB, Eastern Mediterranean Nubian Belt, OF, Owen Fault, WC, Western Caucasus, EC, Eastern Caucasus, EAF, Eastern Anatolian Fault

2. Brief Geological-Geophysical Background

This paper presents an integrated analysis of the North Africa–West Asia region, where giant tectonic plates and several comparatively small tectonic units interact [11]. This region includes numerous active faults and interacting tectonic belts, a complex outline of continental and oceanic crust of different ages, high-intense geodynamic activity, and several high-amplitude gravitational anomalies. Besides this, this region is also characterized by essential seismic velocity deviations registered at the upper and lower mantle, indicating the non-conventional structure at these depths. Zones of the final subduction phases and initial rifting (spreading) stages are relatively closely located in this region [13, 14, 23–26]. The tectonic instability of this region, located in the junction zone between East Gondwana and Eurasia, is determined by the geodynamic intensity of collisional and rifting types (Figure 1). Structurally complex fold belts and cratons have developed, and different geodynamical-physical are manifested [11, 25, 27, 28].

The region is at the boundary planetary zone between Eurasia's two largest plate-tectonic zones and Central Gondwana. The Eurasian segment includes the East European platform, the Late Paleozoic Scythian-Turanian belt, and the Alpine-Himalayan orogenic belt dissected by a fault with residual basins of the Paratethys basin – the Black and Caspian Seas (Figure 1). The southern (Central Gondwana) plate-tectonic segment is composed of the Early Precambrian cratons of the western (Nubian) zone – Saharan, Congo, and Tanzanian and the East Arabian craton (EAC). Between the Nubian zone

and the EAC, a dominant submeridional Neoproterozoic fold-metamorphic belt is developed [13]. Diagonally, this Precambrian structure is dissected by faults of the newest Red Sea rift system.

The youngest mobile belt of the Arabian zone is pre-Cenozoic. It is a fold-block arc of the Mesozoic terrane belt (MTB), deeply advanced to the north into the zone of the Alpine-Himalayan orogenic belt. Its distal part is shown with the corresponding sign (Figure 1). It is significant that in the zone of this joint, the width of the Alpine belt of the Pontic-Caucasian zone is reduced to a minimum – of about 500 km. Furthermore, to the west, from the Cyprus arc to Eastern Crimea, the width of the Alpine belt exceeds 1,200 km.

The analysis of the structural-tectonic position of the Turkish seismic phenomenon is well complemented by the data of supra-regional geodynamic zoning of the transition zone between Eurasia and Central Gondwana (Figure 2).

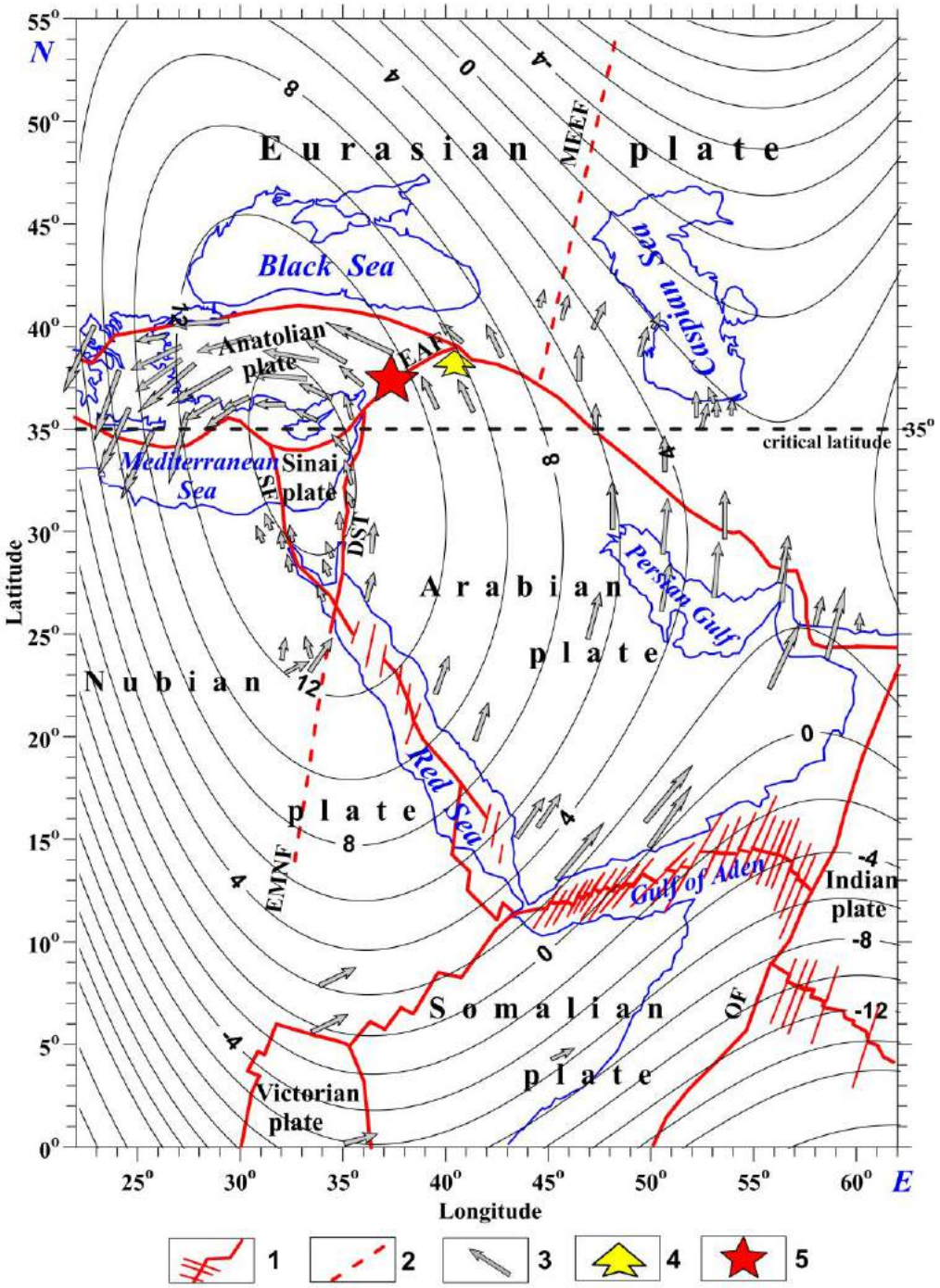

Figure 2. Integrated scheme of geodynamic indicators distribution of the region under study (overlaid by the residual gravity anomalies) (after [16], modified and supplemented). (1) main interplate faults, (2) main intraplate faults, (3) vectors of the GPS monitoring [14, 29, 30], (4) distal part of the Mesozoic terrane belt, (5) high magnitude seismogenic zone in Eastern Turkey (February 06-07, 2023).

Several heterogeneous structures were identified in an extensive zone from 0 to 55° of northern latitudes, at the intersection of which an anomalous seismic zone is located. First, this is the critical parallel of 35°, within which the most intense shifts occur due to the Earth's figure meridian skew [31]. Near this parallel, the junction boundary of Eurasian,

Arabian, Anatolian, Sinai, and Nubian lithospheric plates passes [16]. According to the same work, in the indicated space of the planetary joint, the data on satellite geodesy differ most sharply with the development of an intensive turn of tectonic blocks to the west and southwest in a counterclockwise direction [10, 32, 33].

However, the most crucial feature of the geodynamics of the region, the most essential for understanding the seismic phenomenon under consideration, is the discovery and mapping of an extensive sub-oval structure of the deep mantle, rotating in a counterclockwise direction [15]. The axial part of this structure stretches from SSE to NW, as can be seen from the nature of the location of the isolines of the structure itself (Figure 2). Cyprus is in the center of this mantle structure projection, and the zone of anomalous seismicity in Eastern Turkey is in the zone of transition from the arch of the uplift ENE; this fact is essential for further analysis.

3. Applied Geophysical-Geological Methods

The applied multidisciplinary set of geophysical (satellite, airborne, and surface (sometimes subsurface)) and geological methods is presented below. It should be noted that practically all employed methods are independent, and the data were obtained from different sources. The discovery of an early unknown deep giant target raises the question of the possibility of detecting other similar objects at a depth near the critical latitude ±35º.

3.1. Satellite-derived gravity field analysis

Examination of satellite-derived gravity data is a powerful regional tectonic–geodynamic zonation instrument, including comprehensive tectonic–structural interpretation, data transformation, and segmentation [13, 22, 34–38]. The satellite-derived gravity data for this study were acquired from the World Gravity Data Base as retracked from the Geosat and European Remote Sensing (ERS) missions [e.g., 39]. Eppelbaum and Katz [35] have exposed that to examine the deep structure of large regions (several million km^2 or more), satellite gravity data retracked to the Earth's surface can be employed without any reductions. Eppelbaum et al. [16] have investigated a satellite gravimetric dataset for the region of 0°–55° N and 22°–62° W. This research used the polynomial approximation to recover the nature of anomalous sources, an effective tool for solving various problems in applied sciences (including geophysics) [e.g., 40].

Processing the 'Big Data' satellite gravimetric dataset (more than 9.5×10^6 measurements were used) removes abundant random elements. The residual gravity anomaly attained using the polynomial cubic surface approximation is like the results of nonlinear and distance filtering methods. The primary trend in all the gravity mentioned above map transformations displays a deep oval (quasi-ring) anomaly superficially reflecting a deep target creating this anomaly (Figure 2). It is the standard procedure to analyze quantitatively transformed potential (magnetic, gravity, thermal, etc.) field anomalies [e.g., 20, 41]. The residual gravitational anomaly was interpreted using improved methods of characteristic point, improved tangent, and areal, specially developed to analyze potential geophysical anomalies when the superposition of different anomaly ranks is observed [42]. The depth of the anomalous source is known to be associated with the anomaly's wideness, its branches' inclination, the square occupied by the anomaly area, and some other parameters. Employing these methods specified that the upper edge of the enormous quasi-ring (ellipsoidal) structure occurs at 1650–1700 km in the Earth's lower mantle.

The gravitational attraction of sizeable deep mass (uplift of the more dense rocks) gives rise to stresses in the upper layers of the Earth [43]. When these stresses are joined with the seismologically active faults near (and in) the Earth's surface, a great tension is accumulated that causes preconditions for dangerous geodynamic events.

3.2. Land/marine gravity field analysis

The global geological structure geodynamic analysis testifies that arched zones are mostly unstable segments (in the case of rotation – especially) [43]. An intense trend of the Bouguer gravity anomalies sharply outlines the Red Sea spreading zone [44] (Figure 3c). It agrees with the long axis of the residual satellite-derived gravity map (Figure 3a). At the same time, the high-amplitude Cyprus gravity anomaly [45] (Figure 3b) coincides with the center of the residual gravity anomaly. The map presented in Figure 3c displays that the Bouguer anomalies reach almost +100 mGals in the axial zone of the Red Sea rift, lengthwise the long axis of the revealed structure. Figure 3c agrees with other geological–geophysical data, signifying structure asymmetry and displacements of both sides of this rifting zone in the Red Sea region [15]. Consequently, there was a reliable agreement between three independently observed gravimetric data sets.

Bouguer gravity anomalies in the eastern and western frames of the Red Sea, crosscutting the system of igneous and metamorphic complexes, display regional asymmetry in the gravity field behavior (see Figure 3c). In the west, within the Nubian Plate, the Bouguer anomalies have near-stable platform values: ±50 mGals. In sharp contrast to these data, on the eastern coast (corresponding to the Arabian Plate), the Bouguer anomalies are linearly elongated parallel to the Red Sea coast. Pronounced negative values, typical for activated platforms, characterize them.

The developed satellite-derived gravity gradient map (Figure 4) shows that the seismicity anomalous zone is confined not to the axial zone of the deep mantle structure but to its periphery.

(1) main fault systems, (2) interplate and intraplate faults, (3) Mediterranean Ridge, (4) distal part of the Mesozoic terrane belt, (5) Magnitudes on earthquakes registered 06.02.2023 in Eastern Turkey till 13.15 UTC: a: > 7.5, b ≥ 6.0, c: ≥ 4, d: ≤ 4 (magnitudes after [46] and SCEM DB). ECB, Eratosthenes Continental Block, DST, Dead Sea Transform, SF, Sinai Fault, J-S, Judea-Samaria, A, Antilebanon, NAF, Northern Anatolian Fault, EAF, Eastern Anatolian Fault.

In other words, the gradient gravity map showed the deviation of the seismic zones in the direction to the west of the distal bulge of the Arabian lithospheric plate, i.e., counterclockwise. This follows from the analysis of the gradient data: the Arabian, Sinai, Nubian, and central parts of the Anatolian plate have minimal gradient values, up to 300 arbitrary units, and in the zones of plate junction, they reach a value of 1,000 units, which can be seen in the junction zone of the regional faults DST, EAF, and the Cyprian arc. This additional element of the crust's stressed state is not decisive for determining the genesis of the considered seismic phenomenon but, undoubtedly, can be used if new geological and geophysical data are involved, which will be shown below. The constructed map (Figure 4) precisely agrees with the map of the earthquake distribution (altogether 178 events) registered on 06.02.2023 till 13.15 UTC [46].

3.3. GPS vectors behavior

The GPS pattern reconstructed from [14, 29, 30, 47] unambiguously indicates the visible counterclockwise rotation in the region under study (Figure 2). The distribution of GPS vectors (see Figure 2) agrees well with the residual gravitational anomaly isolines (Figures 2 and 3) and the summarized paleomagnetic vector orientations (Figure 1). It testifies to the presence of the so-called geodynamic vortex structure in the central-western part of the region. The Cyprus high-amplitude gravity anomaly occurs in the center of this structure (Figure 3). However, the GPS vectors gradually acquire a clockwise direction outside the residual gravity anomaly contour, i.e., in the region's northeast (Figure 2). The paleomagnetic vector direction also accompanies this effect, changing from counterclockwise to clockwise (Figure 1).

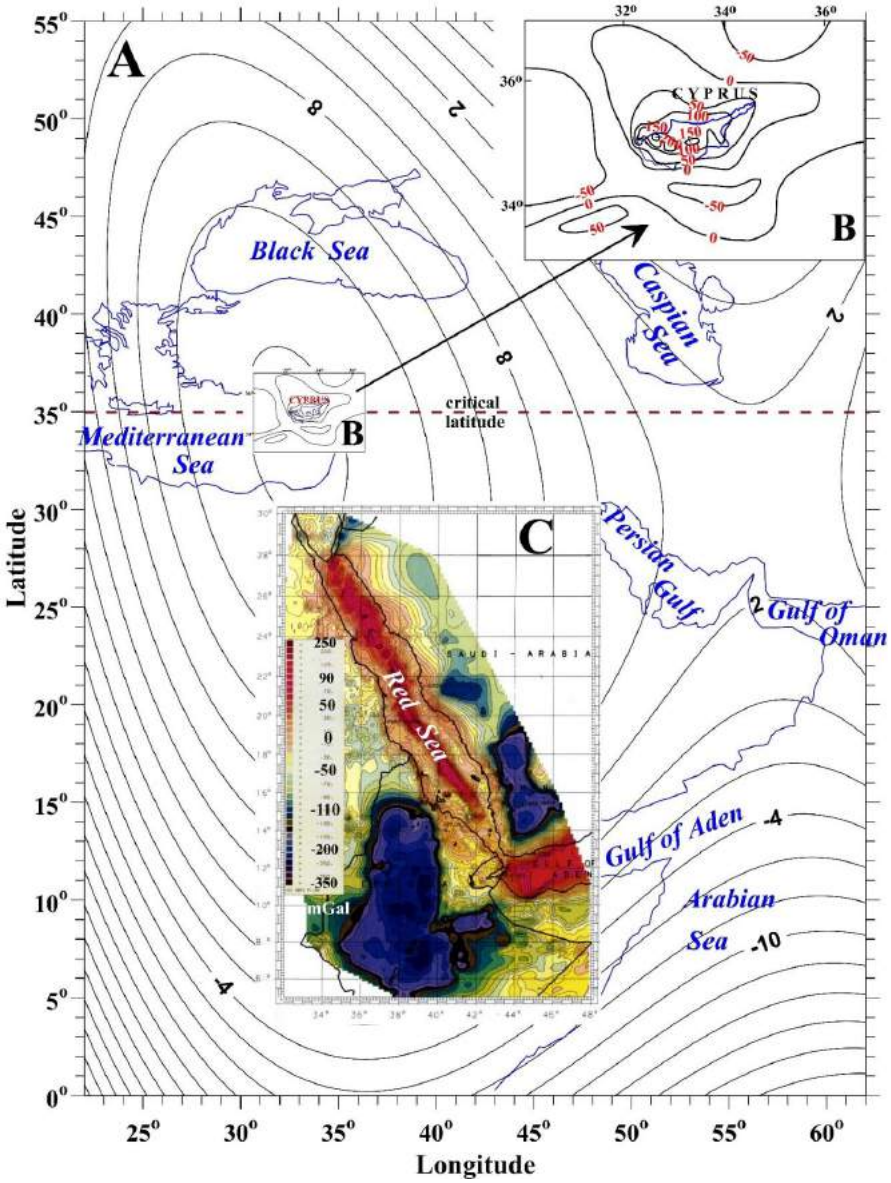

Figure 3. Comparison of gravitational anomalies (modified after [15]): (a) Residual satellite-derived gravity anomaly, (b) Cyprus isostatic gravity anomaly (land/sea) (after [45]); (c) Bouguer anomalies observed in the Red Sea and adjacent areas (sea/land) (after [44]). The dashed line displays the 35° critical latitude of the Earth.

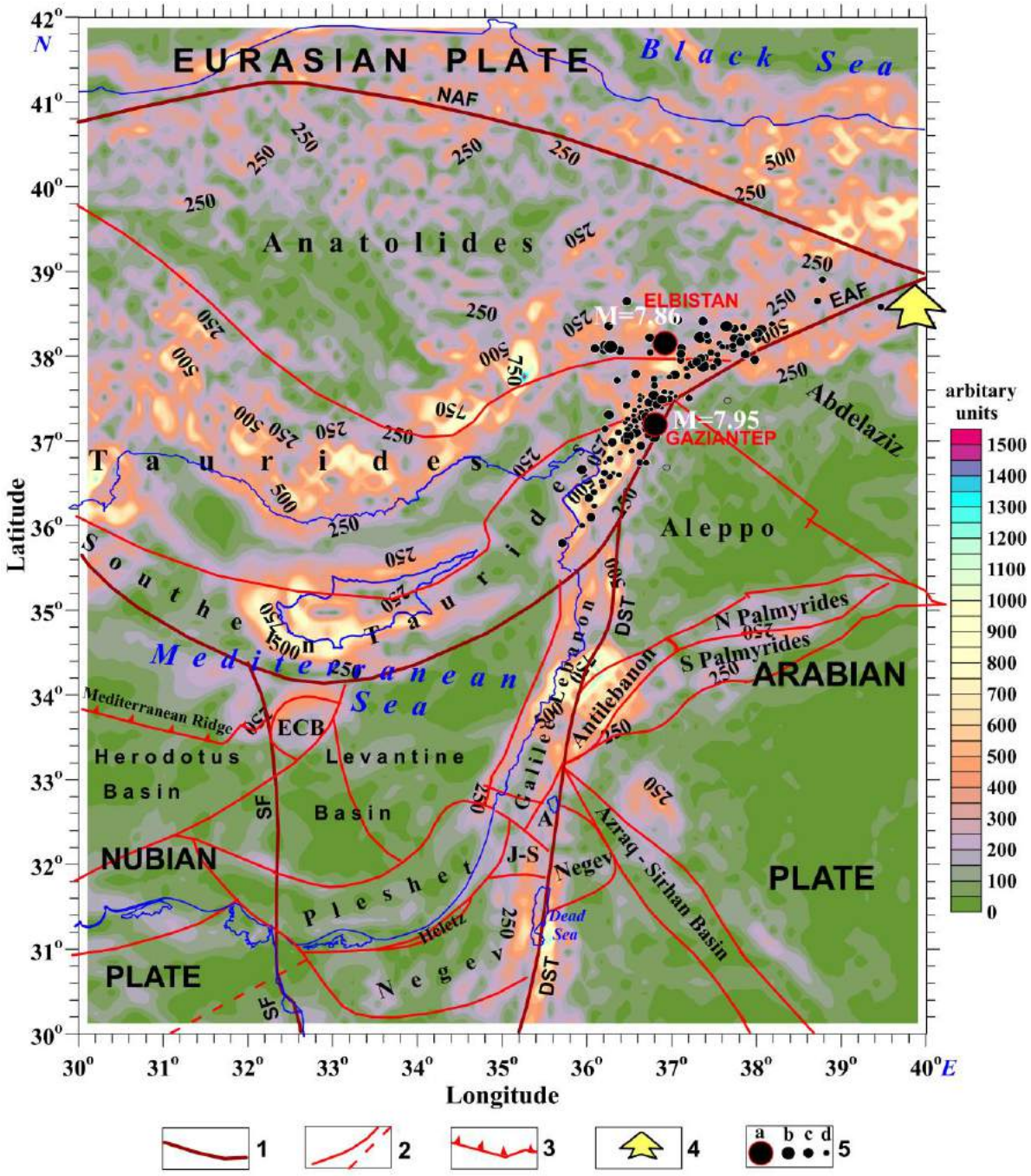

Figure 4. Satellite-derived gravity gradient map with eastern Turkey's main tectonic elements and seismological features. (1) main fault systems, (2) interplate and intraplate faults, (3) Mediterranean Ridge, (4) distal part of the Mesozoic terrane belt, (5) Magnitudes on earthquakes registered 06.02.2023 in Eastern Turkey till 13.15 UTC: a: > 7.5, b ≥ 6.0, c: ≥ 4, d: ≤ 4 (magnitudes after [46] and SCEM DB). ECB, Eratosthenes Continental Block, DST, Dead Sea Transform, SF, Sinai Fault, J-S, Judea-Samaria, A, Antilebanon, NAF, Northern Anatolian Fault, EAF, Eastern Anatolian Fault.

3.4. Map of geoid isolines evaluation

The geoid map reflects integrated effects from the Earth's crust, mantle, and core [48– 50]. The generalized geoid anomalies for the study region (based on the EMG2008 data) and their comparison with the GPS pattern are shown in [16]. The geoid isolines' behavior presents the huge quasi-circular anomaly elevations reflecting the deep ellipsoidal arch structure and lows – his periclinal parts (Figure 5). Geodynamically, this map is consistent well with the GPS vector behavior and the residual gravity field [16]. The geoid anomalies also show a correlation with the primary regional tectonic units. This map markedly indicates the deep origin of the discovered combined phenomenon.

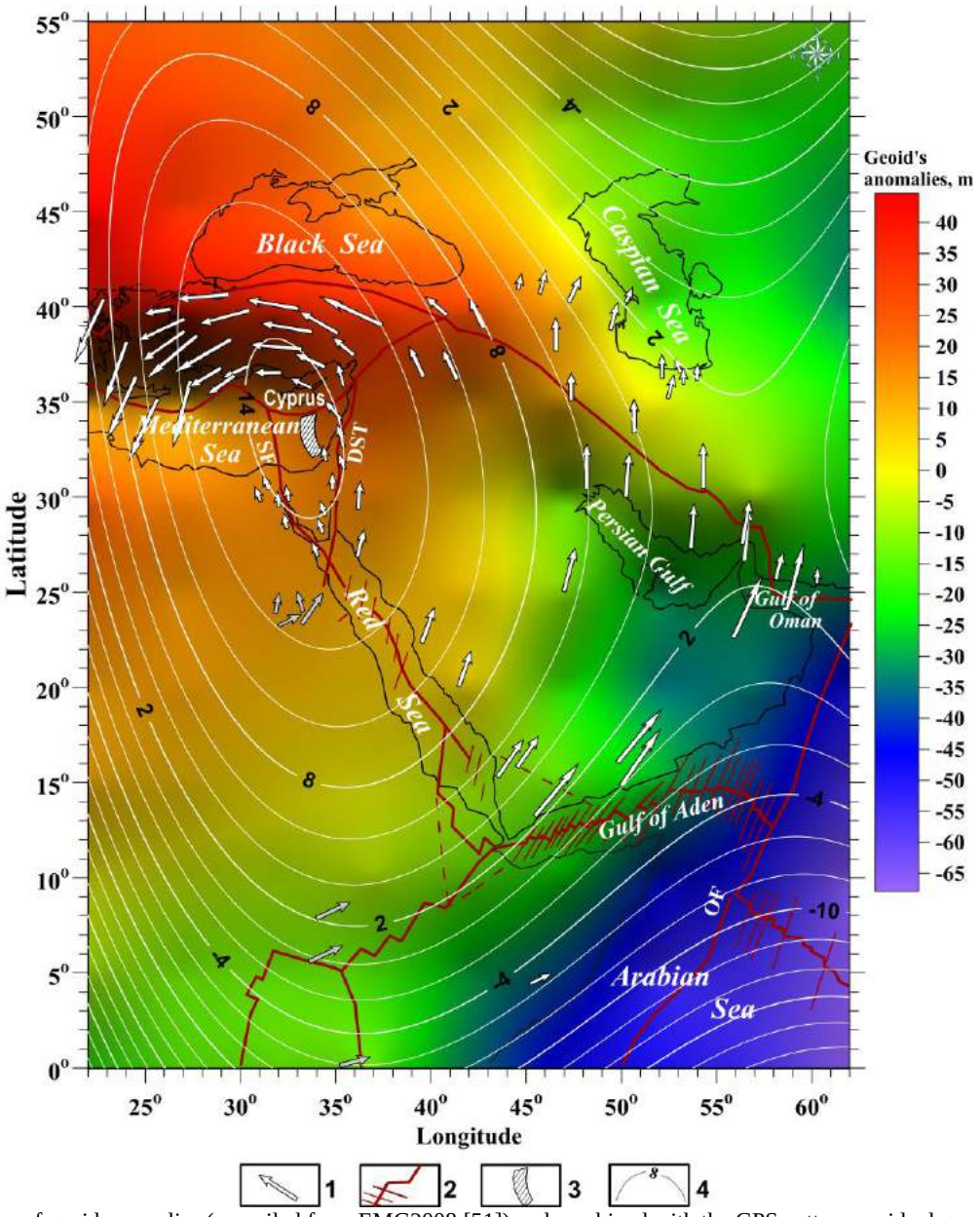

Figure 5. Map of geoid anomalies (compiled from EMG2008 [51]) and combined with the GPS pattern, residual gravity anomaly isolines, and main tectonic elements. (1) GPS vector pattern [14, 29, 30, 47], (2) main interplate faults, (3) Kiama paleomagnetic hyperzone of inverse polarity [22], (4) isolines of the residual gravity anomaly. SF, Sinai Fault; DST, Dead Sea Transform; OF, Owen Fault.

3.5. Paleomagnetic data generalization

It is well-known that paleomagnetic data are the main indicators of tectonic block rotation [52–54]. The examination of the geodynamics in the central part of the projection of the anomalous ellipsoidal deep structure (including the western margin of the Neoproterozoic fold belt, the structural zones of the Eastern Taurides, southern and northern margins of the Mesozoic terrane belt, Cyprus arc, Crete Island, Aegean Sea, and Western Carpathians) indicates that the tectonic block rotation is predominantly counterclockwise (Figure 1) [10, 22, 55–67]. In the Western Caucasus, relating to the peripheral part of the deep structure projection, the prevailing counterclockwise block rotation is observed [e.g., 68–70]. In contrast, in the Eastern Caucasus, located outside the contour of the mantle structure projection, the clockwise rotation of the crustal block has been recognized [55, 68–71] (Figure 1).

Analysis of paleomagnetic data in the peripheral parts of the deep structure projection indicates geodynamic instability. However, paleomagnetic rotations in the central part of the mantle structure projection are mainly counterclockwise (Figure 1) and agree with the counterclockwise GPS vector behavior, the residual gravity field isolines (Figure 2), and geoid anomalies (Figure 5) [16].

In detail, let us consider three typical examples of tectonic block counterclockwise paleomagnetic rotations. For performing optimal paleomagnetic mapping, a suitable classification is necessary. The development of Jalal, Sogdiana, Gissar, Tuarkyr, and Khorezm paleomagnetic arrangement is presented in [72, 73].

3.5.1. Cyprus area

Morris et al. [74] have shown that the ophiolite massifs of Troodos (Cyprus) and Baer-Bassit (Syria) underwent substantial counterclockwise rotation. Paleomagnetic reconstructions enabled the compilation of the geodynamic diagrams demonstrating the counterclockwise rotation of the Cyprus structure from the Cretaceous to the Late Cenozoic (Figure 6).

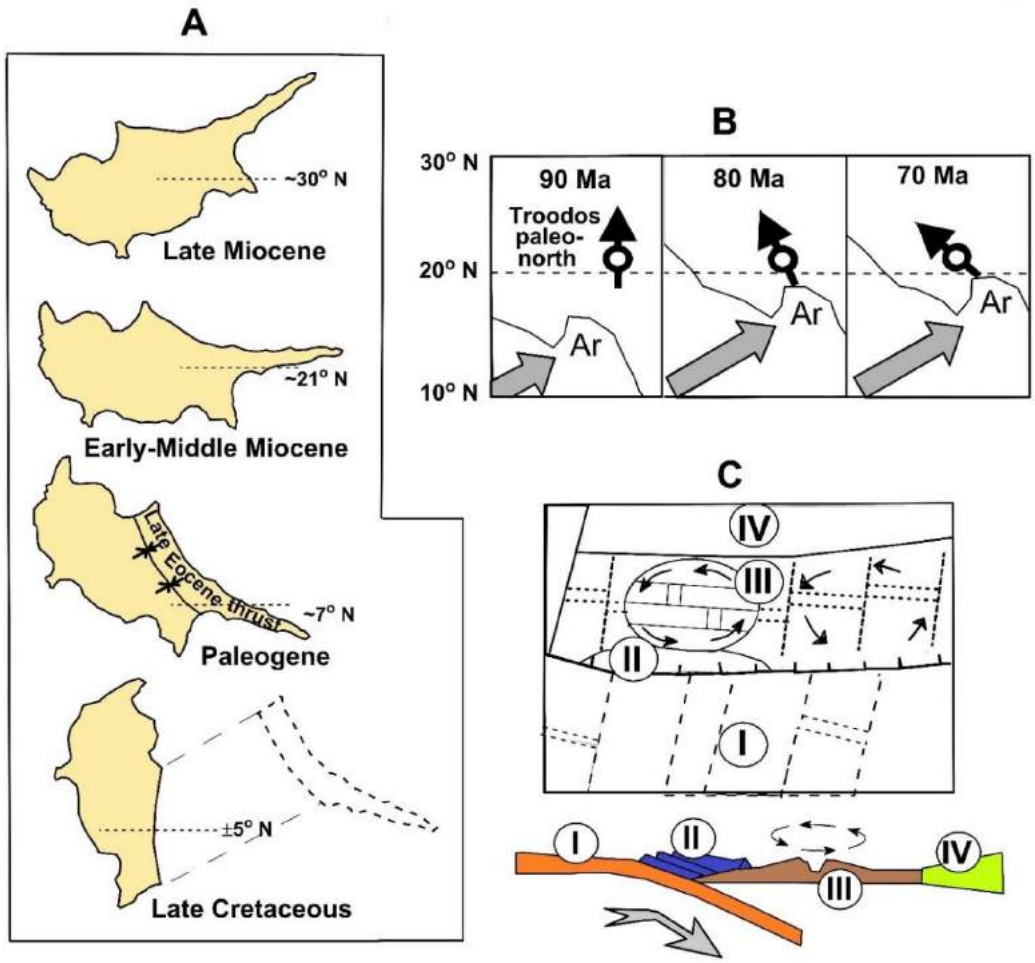

Figure 6. Cyprus geodynamic schemes of the counterclockwise rotation (Cretaceous–Late Cenozoic) (modified after [16]): (A) counterclockwise rotation of Cyprus from Late Cretaceous to Late Miocene (based on the paleomagnetic data from [62]), (B) change in the relative position of Cyprus and the African–Arabian Plate of Gondwana paleocontinent in the Late Cretaceous (based on the paleomagnetic data from [74]), (c) Cyprus paleostructures paleogeodynamic reconstruction of within the Late Cretaceous Tethys Paleo Ocean and its frame (after [75]). Ar, Arabian part of Gondwana. I, subducting oceanic plate of the Neotethys southern side; II, ophiolite complex of the Early Mesozoic crust of Mammonia basin; III, spreading zone of the Late Cretaceous part of the middle Troodos ridge; IV, terrane zone of the Aegean–Anatolian belt with the continental crust.

3.5.2. Makhtesh Ramon area (Southern Israel)

The Makhtesh Ramon terrane (Southern Israel) is the extreme southwestern part of the MTB, collisionally articulated with the Arabian-Nubian part of Gondwana [22]. This fact explains the high complexity of the Ramon subterrane structure, which contains various geological-geophysical tectonic-structural elements. Paleogeodynamic development of this subterrane was formed during the pre-collisional, collisional, and post-collision stages.

The subterrane (Figure 7) has a wedge-shaped outline, the narrowed part of which is in the southwest and extends to the northeast. The paleomagnetic scheme (Figure 7A) and the diagram of the historical and geodynamic reconstructions (Figure 7B) conventionally depict not all subterrane but the outline of its submerged part corresponding to the erosion-tectonic depression, enclosing the Mesozoic outcrops (Lower Cretaceous, Jurassic and Triassic) and Late Cenozoic [76].

These rocks are permeated by a variety of Mesozoic traps, whose radiometric ages range from 165.7 to 93.8 Ma [77] and contain the outcrops of the ophiolite plates of the Saharonim basalts [22], the radiometric age of which is refined within 207 and 205 Ma [78]. They correspond in age to the Illawarra-2 superzone [22], confirming the paleomagnetic studies' data [79] and determining their normal polarity.

In Makhtesh Ramon, we used the analysis of the discontinuities and hypsometry of the plateau framing the canyon itself and outlines of the erosional canyon. The latter is essential because the boomerang-like canyon outlines with a deviation of the southwestern end to the east and northeast – to the west, indicating the counterclockwise rotation of this subterrane. At the same time, the highest hypsometric marks exceeding 1,000 m are in a narrow zone corresponding to the center rotation of the tectonic block. The cirrus nature of tectonic ruptures, spherical in places with prominent shear-slip elements, confirms the regional nature of the rotation of the structure, mainly in the counterclockwise direction. Analyzing the evolution of movements of the Ramon subterrane (Figure 7B) was used to examine the movement of the radiometrically dated dikes and chains of the effusive rocks displaced from the primary latitudinal orientation. The performed studies showed that during almost the entire Jurassic-Middle Cretaceous stage, the area experienced a movement from the Neotethys Ocean's southern side to the southwest with a concomitant counterclockwise rotation (except for a part of the Aptian centuries (125-115 Ma ago), when the sublatitudinal post-collisional dikes shifted clockwise).

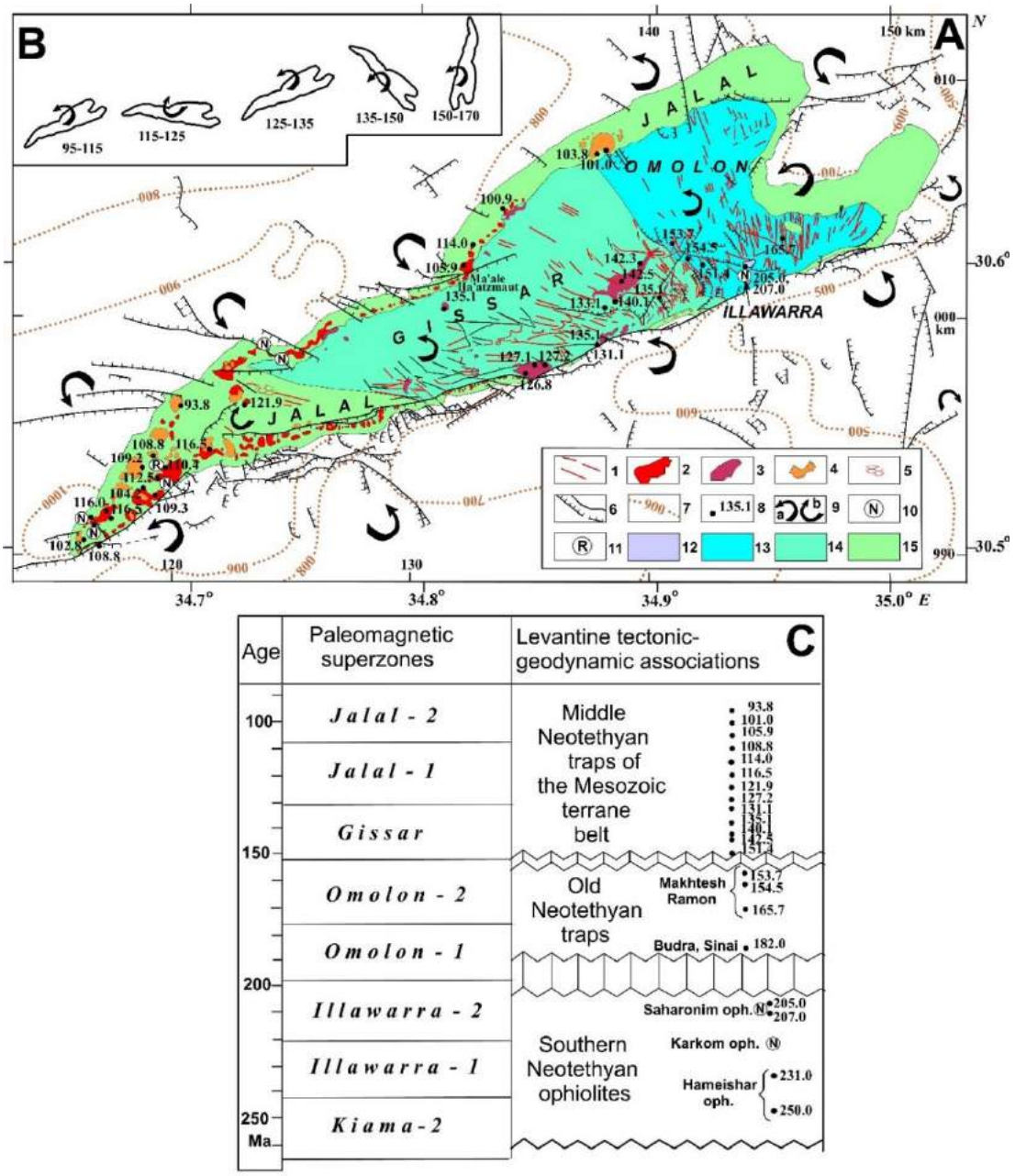

Figure 7. Makhtesh Ramon (Negev Desert, southern Israel) geodynamic-paleomagnetic map (revised and supplemented after [78]). **A**: geodynamic-paleomagnetic indicators. **B**: geodynamic changes of Makhtesh Ramon subterrane displacement in the Middle Mesozoic. **C**: Paleomagnetic scale.

(1) precollisional-collisional basalt dikes, (2) postcollisional alcalic olivine basalt flows and volcanoclastic rocks, (3) precollisional association of alkali olivine gabbro, monzogabbro and syenites, (4) postcollisional association of basanites and nefelinites, (5) quartzitic hexagonal prisms, (6) faults, (7) hypsometric isolines within the Makhtesh Ramon plateau (1-7 from [22, 76, 80–94], (8) radiometric age of the magmatic rocks (from [77]), (9) counterclockwise (a) and clockwise (b) rotation of the linear structures (faults, dykes, and volcanic ridges), (10)-(11) magmatic rocks with normal (10), and reversal (11) paleomagnetic polarity (from [78, 95, 96], (12)-(15) paleomagnetic zonation (classification) of the magmatic complexes: (12) Illawarra, (13) Omolon, (14) Gissar, (15) Jalal.

3.5.3. Hermon area (Northern Israel)

The Hermon Mt., belonging to the Antilebanon terrane, is the most elevated tectonic block of the Easternmost Mediterranean, reaching an absolute elevation of 2,482 m above sea level and with an abnormal increase in the depth of the Moho surface – over 37 km [97]. The paleomagnetic map of the Mt. Hermon area is based on an integration of petrological [98, 99], petrostructural [100], radiometric [98–103], paleomagnetic [102, 104], and some other data (Figure 8A, B, C). All these data enable us to conclude that within the study area, three paleomagnetic complexes are developed, two of which are Mesozoic (Gissar and Jalal), and one is Late Cenozoic; the youngest zones of the Brunhes and Matuyama relate to the Sogdiana superzone (Figure 8C). The most ancient Gissar superzone is in the central and eastern parts of the region and is composed of Jurassic carbonates. Few radiometric age data for the Gissar dikes in the north give estimations of 140, 132.4, and 130 Ma. To the south, the xenoliths of these rocks were carried by younger volcanoes, and their radiometric ages were 16, determined between 150 and 140 Ma. In the Elazar horizon, the age of conglomerates is determined as 146 Ma [99]. These data are in good agreement with the age from the basal part of the Tayasir traps (Wadi Maliah) – 146 and 133.5 Ma [103, 105], and with the age of the Um Sabune Middle Miocene basalt conglomerates, 141.9 Ma in the Shelah area, 35 km north of the Lower Cretaceous' basite outcrop. This tectonic peculiarity is reflected in the inset (Figure 8B), which indicates the counterclockwise rotation of the Antilebanon terrane from the Jurassic to the present time.

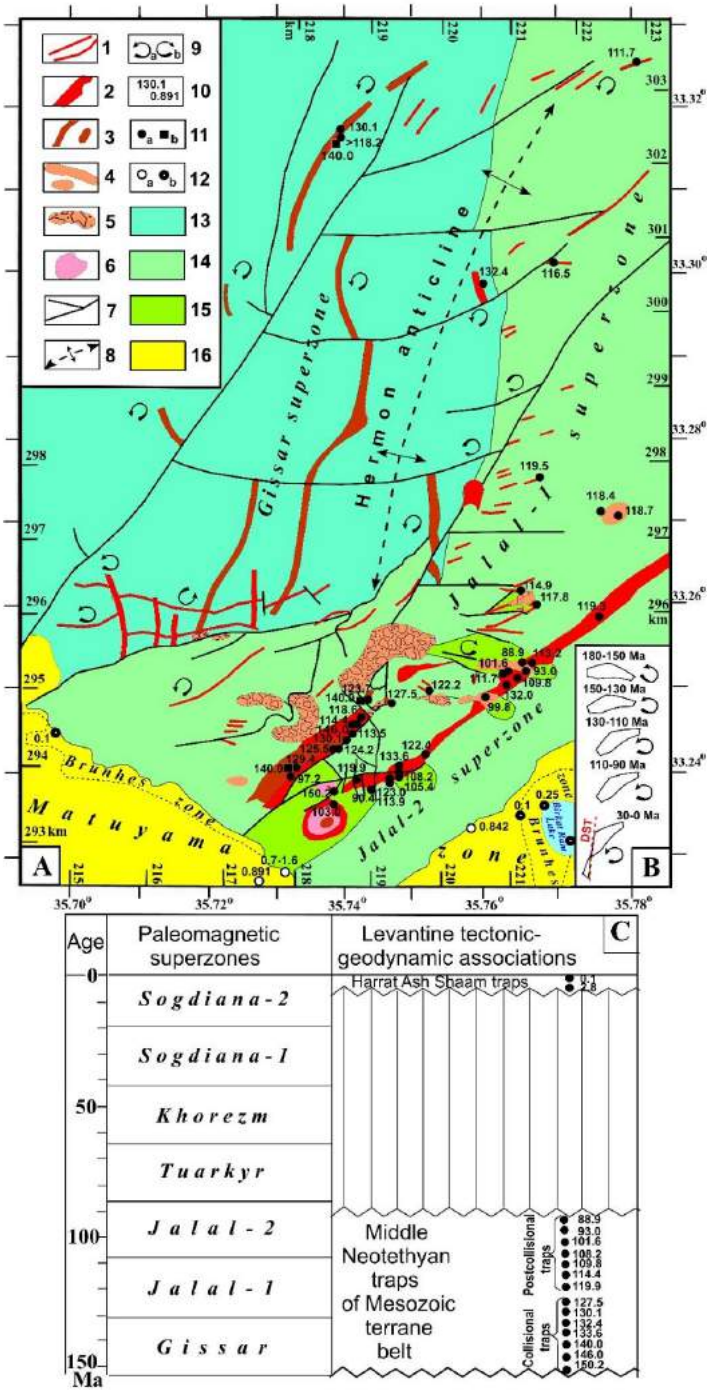

Figure 8. Mt. Hermon geodynamic-paleomagnetic map. **A**: Tectono-paleomagnetic indicators. (1) Lower Cretaceous basalt-basanite dikes, (2) Lower Cretaceous alkaline basalt flows and tuffs, (3) Jurassic - Lower Cretaceous diabase dikes, (4) Lower-Upper Cretaceous alkaline basalt flows, (5) Lower Cretaceous diatreme pipes, (6) Upper Cretaceous alkaline basalt cone, (7) faults, (8) axis of the Hermon anticline, (9) counterclockwise (a) and clockwise (b) rotation of faults and magmatic bodies, (10) radiometric age of magmatic rocks, (11) points of Mesozoic magmatism studied by different methods: (a) by K-Ar, Ar-Ar data, (b) Nd-Sr-Pb isotopic data, (12) paleomagnetic measurements of the Pleistocene magmatic rocks: (a) reverse polarity, (b) normal polarity; ((1–8) and (10–12) from [98–109], paleomagnetic zones (13-16): (13) Gissar, (14) Jalal-1, (15) Jalal-2, (16) Sogdiana-2 (Matuyama and Brunhes Chrons). **B**: geodynamic changes of Antilebanon terrane displacement in the Middle Mesozoic – Cenozoic. **C**: Paleomagnetic scale.

3.6. Critical latitude of the Earth

Véronnet's [31] comprehensive physical-mathematical analysis of the Earth's rotating ellipsoid indicated that the two Earth's critical latitudes are ±≅35°. These effects are due to the Earth's rotation velocity changes and the tidal forces' uneven impact. Further studies using extensive geological-geophysical materials demonstrated that, following Véronnet's theory, periodic matter fluxes in the Earth's mantle move from the equatorial to the polar regions and vice versa [110, 111]. Eppelbaum et al. [16] showed that the latitude of +35° coincides with the center of the projection of the revealed quasi-circular mantle structure (Figure 2).

3.7. Results of regional seismic tomography studies

The results of deep seismic tomography [112–118] testify to abnormal velocities of P- and S-wave propagation at depths of 1400–1750 km beneath the Eastern Mediterranean that also confirm the existence of the giant anomalous target in the lower mantle. The seismic tomographic profile through the Antalya region at 40° N (southern Turkey) indicates heterogeneous sources in the mantle indoors, the contour of the recognized huge quasi-ring object at depths of about 1600 km [117].

Recent regional seismotomographic studies using global P- and S-wave models [118] confirmed the presence of a deep anomaly within the projection of the mantle structure (see Figures 2 and 5 in the present paper). According to profile D-D' data [118], its surface plunges from SW to NE at depths from 1,600 to 2,000 km from the southern part of the Red Sea to the northern part of the Persian Gulf (Figure 9 in [118]. According to the more northern profile A-A' (Figure 8 in [118]), this surface is subducted from west to east from the Anatolian block (Turkey) to the Zagros Mts. (Iran) from the depths of 1,200 to 2,000 km. The data from this deep profiling entirely coincides with the topological parameters of the previously identified regional gravity residual anomaly [16].

3.8. Study of paleobiogeographical data

Examining paleobiogeographic data confirms deep structure rotation and its relationship with near-surface structures. Like the paleomagnetic ones, they show earlier stages of deep structure rotation and its reflection in surface geology. The region under consideration is essential for analyzing the spreading stage of development (mainly Mesozoic) of the development of the Neotethys Ocean and adjacent parts of Gondwana and Laurasia. Special attention is drawn to anomalous biogeographic indicators, particularly shell remains of giant brachiopods *Septirhynchia–Somalirhynchia* [16].

The biogeographical mapping was based on the works of Scotese [119, 120] and the authors' previous investigations [22]. In the region under study, three paleobiogeographical provinces [121–127] were recognized (Figure 9): Boreal (Eurasian shelf), (2) Mediterranean (Mediterranean Basin), and (3) Ethiopian (South Africa). The constructed map (Figure 9) shows the phenomenon (see the red arrow rotating counterclockwise) of the geodynamic transfer of tectonic blocks with the remains of the Ethiopian fauna from the present position of the Persian Gulf to the Levant up to the Egyptian Eastern Desert. This fact proves the counterclockwise movement of the eastern and central parts of near-surface projections of the anomalous deep structure in the Jurassic and Early Cretaceous [128].

3.9. Mineral-petrological analysis

An overview of the mineral-petrological features of deep origin for the study region indicates that many different magmatic indicators are revealed within the projection of the mantle structure. The largest number of rocks and minerals of the deep origin are concentrated in the apical part of the projection. The Cyprus ophiolite zones occur in the center of this area. Numerous mantle minerals were discovered here (e.g., melilite, clinopyroxene, amphibole, olivine, Cr-spinels) [e.g., 129–131]. The mantle rocks and minerals were identified in Eastern Turkey (e.g., REE concentrations, diamonds, mantle peridotites, and harzburgites) [132, 133], western-northern Syria (diamonds and kimberlites) [134], Carmel area (northern Israel) (e.g., ultramafic xenoliths, corundum xenocrysts, mantle peridotites, tistarites, diamonds, moissanite, eclogites, garnet websterites) [135–140]; Makhtesh Ramon area (southern Israel) (e.g., moissanite, corundum, diamonds, olivine, perovskites, yttrium phosphate) [89, 90, 94, 141, 142]; Central Eastern Desert of Egypt (diamonds, some satellite minerals, and kimberlites) [143].

3.10. Magnetic field analysis

Analysis of the GPS local measurements (Figure 2) and paleomagnetic mapping data (Figure 1) made it possible to establish that the deep mantle structure experiences counterclockwise rotation unambiguously [16]. Of course, these data are not based on regional mapping but on disparate data from different parts of a vast sub-oval structure. At the same time, satellite gravimetry data made it possible, on the one hand, to outline the deep mantle oval and reveal the local structures of the Mesozoic terrane belt and other elements of the tectonosphere [16].

Mainly by magnetic and paleomagnetic data analysis, in the central zone of the deep structure projection, the block of ancient oceanic crust of the Kiama hyperzone was discovered [21, 144], and active geodynamics to the north of it in the Cyprus region [16, 22]. However, these disparate data are significant regarding local shifts and need to provide information about the regional turn of the structure itself. The constructed smoothed map of the magnetic field vertical component ΔZ (Figure 10) made it possible for the first time to cartographically show the reality of the apical center rotation in the axial zone of the deep mantle structure of the Eastern Mediterranean. Here is a good coincidence of regional magnetization zones with gravity isolines of the quasi-ring deep mantle structure. The magnetic map indicates that the most prominent stress zone is in southeastern Turkey, near the transition of the apical uplift to the wing of the deep structure projection (Figure 10). It can be seen that the residual gravity anomaly, GPS vector behavior, and the magnetic field pattern create a single ensemble. A zone of slightly increased values of the geomagnetic field anomaly with a gentle central trough is developed here. Furthermore, on the periphery of the central uplift, scattered troughs are discordant concerning the tectonosphere pattern with negative magnetic anomalies.

Figure 11 displays the magnetic map of the Eastern Mediterranean (this map's coordinates are white contoured in Figure 10 and coincide with the gravity gradient map presented in Figure 4). Particularly significant is the fact that in the

negative anomaly of Anatolides- Aleppo, there are zones of manifestation of recent catastrophic earthquakes. The discordance of concentric magnetic anomalies concerning the structures of the Mesozoic terrane belt, Arabia, and Anatolia indicates their connection with deep geodynamics. In this regard, the deep tectonic-geodynamic boundary between Eurasia and Gondwana in the North Anatolian Fault (NAF) region is significant for confirming counterclockwise movements of the deep mantle structure. As can be seen from the data on the northwestern end of the map, the most significant positive anomaly, 90 nT, turns to the southwest, which entirely coincides with the regional GPS data (Figure 2).

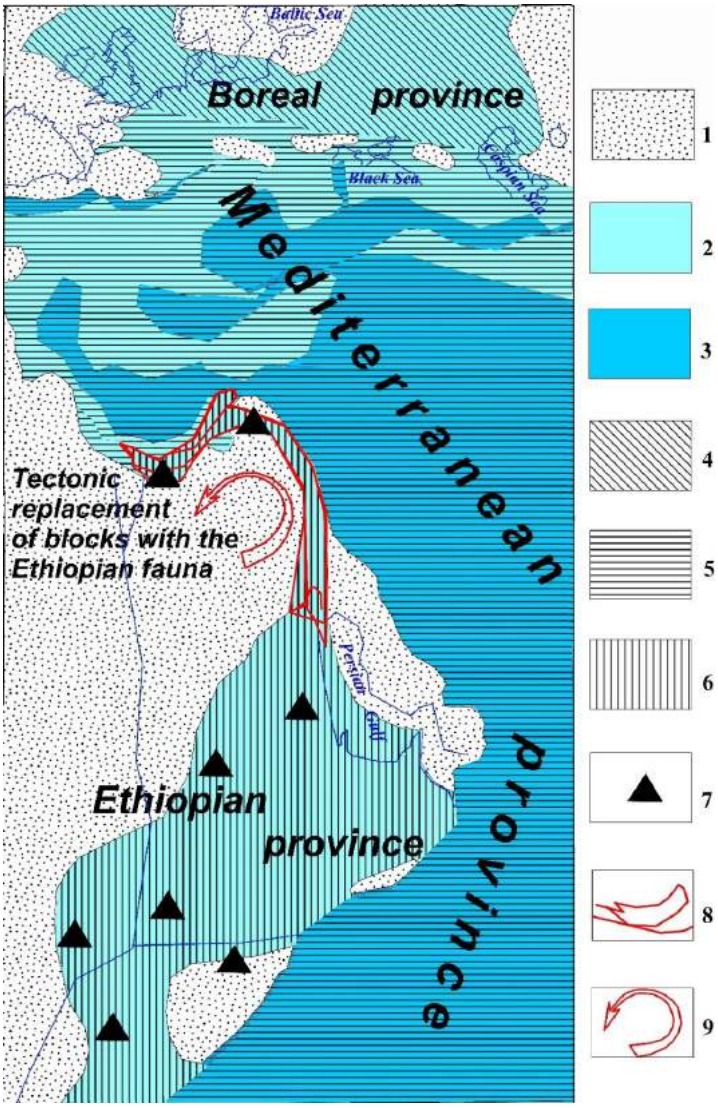

Figure 9. Schematic Late Jurassic paleobiogeographical map of the transitional region of Eurasia and Gondwana with elements of the subsequent Early Cretaceous geodynamics of the Mesozoic terrane belt (when constructing this map, data from [22, 119–127] were used). The solid blue lines show boundaries between seas and land.

(1) land, (2) continental shields and arcs, (3) oceanic plateaus and rifts, (4) Boreal paleobiogeographic province, (5) Mediterranean paleobiogeographic province, (6) Ethiopian paleobiogeographic province, (7) points with Ethiopian brachiopods *Septirhynchia-Somalirhynchia, (*8) tectonic lines of discordant paleobiogeographic replacements, (9) counterclockwise rotated tectonic blocks.

Thus, the foreland sediments of Northern Arabia and Eastern Nubia are tectonically discordantly connected to the allochthonous Mesozoic terrane belt, which rotated counterclockwise in the direction of the paleocontinent Gondwana. This makes it possible for the first time, using geophysical and geodynamic characteristics, to explain the uniqueness of the biogeographically anomalous zone of terrane block attachment to the Gondwana paleocontinent in the middle of the Early Cretaceous in the Levantine phase of tectogenesis [22].

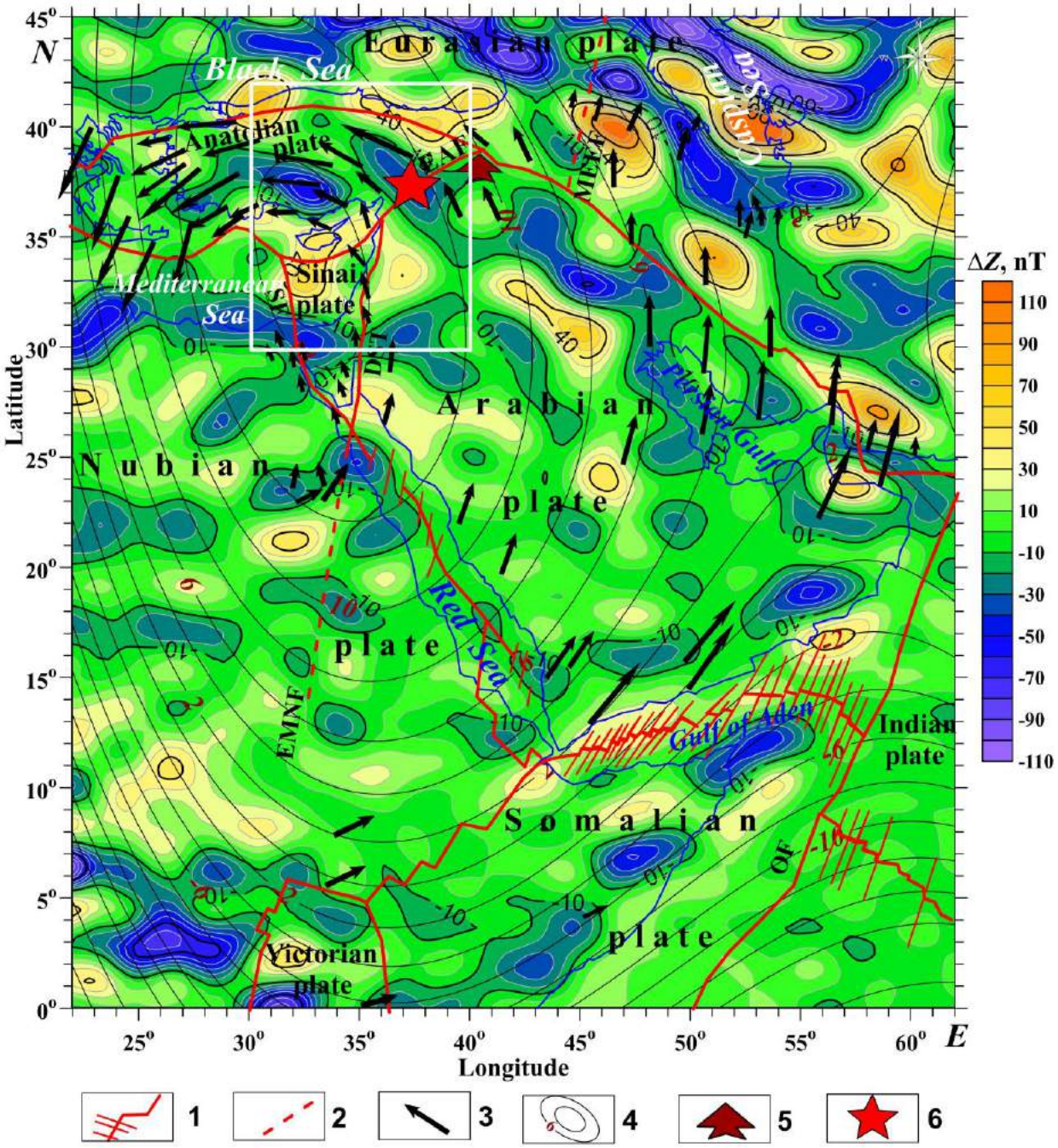

Figure 10. Smoothly averaged magnetic ΔZ map recalculated to one common level of 2.5 km over the msl (initial data from https://geomag.colorado.edu/magnetic-field-model-mf7.html) for African-Arabian region with the main tectonic elements, the behavior of the GPS vectors and overlaid residual gravity anomaly (see Figure 2). The white rectangle contours the ΔZ magnetic map of the Eastern Mediterranean presented in Figure 11. (1) intraplate faults, (2) interplate faults, (3) GPS vectors, (4) residual gravity field isolines, (5) distal part of the Mesozoic terrane belt, (6) epicenters of two main catastrophic earthquakes in Eastern Turkey (February 06, 2023).

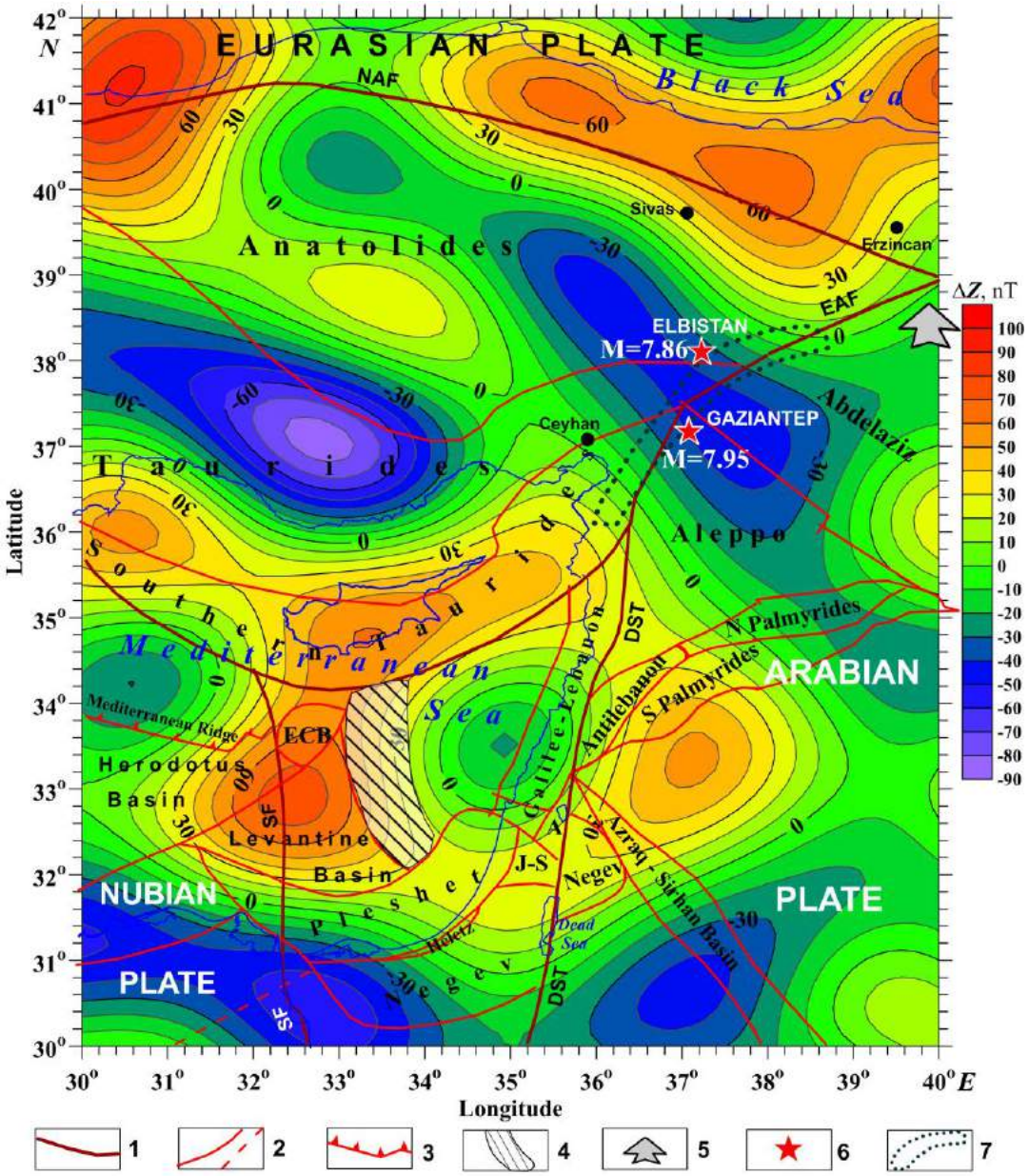

Figure 11. Smoothly averaged magnetic ΔZ map recalculated to one common level of 2.5 km over the msl for the central part of the Easternmost Mediterranean (initial data are from https://geomag.colorado.edu/magnetic-field-model-mf7.html) with the main tectonic elements and seismological features in Eastern Turkey. The contour of this map is shown in Figure 10 by a white rectangle. (1) interplate faults, (2) intraplate faults, (3) Mediterranean Ridge, (4) contour of the oceanic crust block relating to the Kiama paleomagnetic hyperzone of inverse polarity, (5) distal part of the Mesozoic terrane belt, (6) epicenters of two main catastrophic earthquakes in Eastern Turkey, (7) dangerous seismogenic zone (after [145]). ECB, Eratosthenes Continental Block, DST, Dead Sea Transform, SF, Sinai Fault, J-S, Judea-Samaria, A, Antilebanon, NAF, Northern Anatolian Fault, EAF, Eastern Anatolian Fault.

3.11. Asymmetry of sedimentary basins

Ben-Avraham [146] and Smit et al. [147] analyzed the asymmetric basin developments along transforming continental faults on the eastern side of the revealed deep structure projection. Based on our data, the recognized deep structure influenced the asymmetric structure of these basins and their left-lateral regional counterclockwise rotation. Three deep-water trough systems have developed from south to north in the Gulf of Aqaba. They have the form of a series of en-echelon troughs and shift from east to west. This arrangement suggests a combined influence of the shear mechanism and counterclockwise block rotation.

In the Dead Sea region and the Eilat graben system (Israel–Jordan), the axial part of the graben is confined to the east, while its flattened part extends to the west [146–148]. The tectonic-geomorphological and magmatic asymmetries of the Dead Sea basin's eastern and western coasts are well known. Higher amplitudes characterize the eastern part of the basin and are more active [147]. Based on the general gently arcuate structure of the Dead Sea Transform (DST) [146, 149], a new geodynamic concept was proposed to clarify the asymmetry of the deep displacement of the graben-like structures

[16]. It consists of the simultaneous development of shear and rotational displacements of tectonic blocks, which is essential for explaining the regional basin asymmetry.

Lake Kinneret (Sea of Galilee) is located on the DST northern continuation. The lake's deep-water basin axis was displaced to its eastern shore, while the shallow-water basin axis was moved to the western shore. The analysis of paleomagnetic data [150] obtained from areas adjacent to the Galilee region [151] and the results of structural mapping indicate the extensive developments of arcuate faults in the shear zone [146]. It enabled us to illuminate the general dominant nature of the regional movement geodynamics. They are joined with the counterclockwise axial rotating the Arabian–Nubian continental crustal blocks, which agree well with the GPS vector behavior. The asymmetry of local sedimentary basins is also accentuated by the geomorphological asymmetry features of the Arabian–Nubian zone of Gondwana in the Late Cenozoic. In its western part (corresponding to the Red Sea rift zone and Nubian Plate junction), the hypsometric marks of the plateau and Nile River valley commonly do not exceed 500 m. In the eastern part (Arabian–Sinai zone) of the junction of the Nubian Plate with the Red Sea rift zone system and Dead Sea shear zone, the hypsometric marks exceed 500–1,000 m. In the marginal zones of the Arabian and Sinai plates, a mountain range with heights of more than 2,000–3,000 m has formed. We suggest that the described phenomenon of regional geomorphological asymmetry on two sides of the Red Sea rift zone and some other areas is mainly geodynamically caused by the region's counterclockwise rotation.

The concept of the asymmetry of the basins in the Arabian Plate is confirmed by the phenomenon of structural-geodynamic asymmetry in the rift systems in northeastern Africa [152], which are also under the influence of the giant mantle structure (see Figure 2). Here, gentle structures were identified on the eastern and northeastern sides of the rifts and steeper deep reverse faults on the western and southwestern sides of the continental rifts.

3.12. Explanation of the oceanic crust block origin relating to the Kiama paleomagnetic hyperzone

The central part of the Easternmost Mediterranean coincides with the central part of the mantle structure projection and is also associated with low regional heat flow values (~25–30 mW/m^2) [153, 154] (Eppelbaum et al., 2015). This effect reflects the ancient lithosphere age in the studied region [35]. Besides this, the low heat flow may be partially conditioned by the phenomenon of the rotated geodynamic vortex [15], which can cause some heat flow to decrease in the center of the rotated mantle structure [155]. The uniqueness of this zone is accentuated by the detecting (based on the mutual analysis of numerous geophysical-geological data) one of the most ancient oceanic crust blocks relating to the Kiama paleomagnetic hyperzone of reverse polarity (Late Carboniferous–Early Permian) [21, 144] (Figure 11). The upper edges of this block lie at the depths of about 10–11 km at the center of the deep structure projection, a few tens of kilometers south of Cyprus Island [21] (Figures 1 and 11). The occurrence of the strongly magnetized Earth's crust block with reverse magnetization between the positive and negative magnetic anomalies in the magnetic map (Figure 11) is explained as a composite combination of inverse magnetization with a complex geometrical form of this block. The primary formation of the Kiama hyperzone block [22] could have occurred east of the Persian Gulf's present position [75]. Our geodynamic model suggests that this tectonic block was displaced along regional transform faults to its current position under the influence of the deep structure counterclockwise rotation [128].

It should be noted that the allochthonous terrane of the oceanic crust of the Levant, containing the submeridionally oriented paleomagnetic Kiama-Gissar hyperzones, is discordantly associated with the sublatitudinal structures of the south of the Anatolian Plate and blocks of thinned continental crust of the Sinai Plate's central zone. At the same time, the oceanic crust block is very similar petrologically to blocks of the continental crust of the Negev, Heletz, and Galilee-Lebanon terranes, where pre-collision intrusive traps of the Kiama hyperzone are widely developed. In South Sinai, local intrusions of the same age are known [144]. This is because continental and oceanic terranes belonged to both the same stage of tectonothermal activation and were located near the same zone north of the Arabian platform in the area of the modern Persian Gulf. Here, the Neo-Tethys oceanic crust formation began, and movements activated with the subsequent terrane drive to the west in a counterclockwise direction [128]. This formed the arc-shaped block structure of the Mesozoic terrane belt by the middle of the Early Cretaceous. The phenomenon of this movement has been well studied in paleomagnetic mapping of trap complexes associated with the Late Paleozoic-Mesozoic stage of plume activation in the deep mantle structure [144]. It can be proposed that the crucial impact of the deep rotating structure just prevented the oceanic crust block's subduction and preserved its current location.

4. Brief description of the catastrophic seismic events on 06.02.2023 in Eastern Turkey

Many authors have analyzed extreme seismological events in the Eastern Mediterranean and around it [e.g., 17, 18, 29, 35, 139, 156–166]. Numerous researchers investigated the tectonic-geodynamic pattern of the East Anatolian Fault [e.g., [7, 10, 26, 165, 167–169].

The two most decisive dangerous geodynamic events with magnitudes of 7.95 and 7.86 were registered for 9 hours on 06.02.2023 in Eastern Turkey at depths of 18 and 10 km, respectively. These strong events were followed by more than 10,000 significant aftershocks. The mentioned high magnitudes, accompanied by the greatest number of aftershocks, are indicators of the extreme tension accumulated in the upper part of the Earth's crust of the region. Historically, the Mw 7.95 earthquake was the largest in Turkey, exceeding the 1939 Erzincan earthquake of M_w 7.8 [166].

Considering the recent geodynamic past of the Anatolian region, we can see that seven strong earthquakes (M > 6.8) occurred in the North Anatolian Fault (which is also in the dangerous subsurface seismogenic zone and under the influence of the deep mantle structure) during the geologically short period from 1789 to 1905 [169].

4.1. Short seismological-tectonic sketch

Several authors indicated the significant accumulated stress in this area [e.g., 17, 18, 61, 156, 157, 159, 161, 163]. The latest catastrophic earthquakes in Eastern Turkey require their geodynamic understanding. The two most decisive events (with magnitude (M) = 7.95 and 7.86) (according to the last USGS estimations [170] were observed with an interval of 9 hours on February 06, 2023, followed by a whole series of aftershocks (four with M ≥6, about forty with M ≥ 5, and more than 200 with M ≥ 4). The ground acceleration values recorded in some areas near the fault rupture exceeded 1g [171] and even 2g [172]. That is, the amplitude of these catastrophic earthquakes was even higher. These geodynamic events were the most enormous Turkish earthquakes in over 2,000 years [166]. According to Karabulut et al. [7], catastrophic earthquakes were preceded by long seismic silence. This fact indicates a long-term accumulation of seismic stress.

These tragic events led to the death of about 60 thousand people. The above values indicate the colossal tension created in the Earth's crust. The region where these strongest earthquakes occurred is a tectonically complex junction zone of four tectonic plates: Eurasian, Arabian, African, and Anatolian. The joint movement of these plates (consisting, in turn, of tectonic elements of different ages) occurs at an average rate of 6–15 mm per year. However, after two marked powerful shocks, the Anatolian plate shifted to the southwest by three meters; later, this shifting continued for several (entirely to ~11.5) meters.

4.2. First event of M = 7.95, 06.02.2023

The epicenter of this event at (01:17 UTC) was 37 km west–northwest of Gaziantep (Figure 4) and had a maximal Mercalli intensity of XII. According to the United States Geological Survey (USGS), the earthquake hypocenter was at a depth of 10.0 km. The shock had a focal mechanism for strike-slip faulting [172].

A source model for the M = 7.95 seismic event produced by the USGS from observed seismic waves, considering preliminary rupture mapping from satellite data, employed three fault segments. These segments have individual lengths (a), widths (b), strikes (c), and dips (d). Segment 1: (a) >40 km, (b) 30 km, (c) 028°, (d) 85°, Segment 2: (a) >175 km, (b) 30 km, (c) 060°, (d) 85°, Segment 3: (a) >160 km, (b) 20 km, (c) 025°, (d) 75°. The mainshock produced a maximum slip of 11.2 m along segment 2, beneath the Sakarya district in Kahramanmaraş Province, northeast of the junction where it meets segment 1 [172].

4.3. Second event of M = 7.86, 06.02.2023

The first event was followed by M = 7.86 earthquake at 10:24 UTC 95 km north-northeast (Figure 4). It had a depth of 7.4 km, according to the USGS. The shock was also the result of strike-slip faulting [173]; it had an epicenter north of the previous large earthquake (Figure 4).

The USGS source model for the M_w 7.86 earthquake that struck nine hours later has three large fault segments. Segment 1: a >70 km, b > 20 km, (c) 276°, and (d) 80°, Segment 2: a >40 km, b >20 km, (c) 250°, (d) 80°, and Segment 3: (a) ~80 km, b >20 km, (c) 060°, and (d) 80°. The maximum displacement registered on Segment 1 was 11.4 m [173]. Mikhailov et al. [174] even note the displacement on 12.7 m southwest.

4.4. Main tectonic consequences

Thus, the Eastern Turkey land segments were displaced southwest to the Mediterranean Sea (with the maximal movement of 11.2 and 11.4 m (12.7 m?)), i.e., counterclockwise. This fact agrees with the proposed theory about the influence of the counterclockwise rotating deep quasi-circular structure on near-surface geodynamics. The earthquakes' large magnitudes and significant aftershock number (>10,000) point to the greatest accomplished tension in this region. Several scientists [e.g., 161] have noted the significant stress accumulation and increased seismic risk in eastern Turkey.

5. Discussion

Considering that we have different data kinds, we attempted to divide them into three groups (as much as possible): (1) geophysical, (2) tectonic-geodynamic and geological-petrological, and (3) mathematical. At the end of this Section, a combined table is presented.

5.1. Geophysical data analysis

Geophysical-geodynamic mapping (Figures 1 and 2) using tectonic modeling, GPS data analysis [e.g., 14], calculation of a residual satellite gravity anomaly together with the analysis of numerous paleomagnetic (Figures 1 and 6–8), structural-tectonic, petrological, paleobiogeographical (Figure 9), and other data only recently made it possible to obtain a reliable explanation of the geodynamic features and history of the development of the region under consideration [16]. A set of geological-geophysical features revealed a deep mantle structure rotating counterclockwise. In the present paper,

this set is extended and supplemented. This phenomenon significantly influenced all geodynamic regional processes in this most complex region, including dangerous geodynamic events. Interestingly, the tectonic map [7] developed for the Easternmost Mediterranean and Southern Turkey reflects a quasi-circular pattern.

The GPS vector distribution (Figure 2), which unmistakably indicates the counterclockwise rotation, agrees well with the residual gravity anomaly isolines (Figure 2) and testifies to the presence of the geodynamic vortex phenomenon in the Easternmost Mediterranean [15, 36], . The residual satellite gravity anomalies and gravity anomalies observed in Cyprus Island and around it (at the geometric center of the mantle structure projection) and in the Red Sea rift zone (lengthwise the long axis of the mantle structure projection) perfectly match with each other (Figure 3). The Cyprus high-amplitude gravity anomaly [175] occurs at the center of this vortex structure (Figure 3). Meanwhile, outside of the residual gravity contour, e.g., in the northeast of the region, the GPS vectors by degrees obtain a clockwise direction (Figure 2). The paleomagnetic vector directions also accompany this trend, changing from counterclockwise to clockwise (Figure 1).

The regional paleomagnetic data (Figure 1), paleomagnetic sketch map (Figure 6), and paleomagnetic-geodynamic maps of well-studied Makhtesh Ramon (Figure 7) and Hermon (Figure 8) areas unambiguously signify the counterclockwise rotation of tectonic blocks in the deep quasi-ring structure projection. This rotation confirms numerous paleomagnetic studies of the Anatolian block and Western Greece [e.g., 10, 57, 61, 65, 176–179]. At the same time, the geodynamic instability happening in the peripheral areas of the region causes the appearance of both clockwise and counterclockwise rotations. Outside the mantle structure projection, the clockwise rotation prevails.

Eppelbaum et al. [13] developed a map of the thicknesses of the most gravitating surface for the studied region. The depth increasing is displaced to the east in the direction of the deep structure counterclockwise rotation to the central region of the Arabian Plate, with a maximum depth of ≥150 km in the frontal zone of the mass's deep movement [13]. The minimal depth (~70–75 km) outlines the eastern coast of the Red Sea and the zone east of the DST that generally coincides with the mantle structure's long axis.

The first compiled maps of the vertical magnetic component ΔZ (Figures 10 and 11) noticeably display a circular behavior of magnetic anomalies in the corresponding regions. Such behavior is an additional solid argument confirming the influence of the rotated mantle structure. These maps indicate the influence of a deep anomalous object on the rocks occurring at depths of no more than several tens of kilometers (for instance, for Israel, the calculated depths to the Curie discontinuity range from 38 to 46 km [144]).

The generalized geoid anomaly map (Figure 5) represents a large quasi-ring anomaly that correlates well with the residual gravity anomaly map and GPS vector distribution (the last two features are shown in Figure 2).

Platzman et al. [57] asked, "Why are there no clockwise rotations along the North Anatolian Fault Zone?" There were no physical-geological models to answer this question since these models were developed relatively recently [15, 16]. This answer is obvious: counterclockwise rotation of the deep structure generates a specific stress on the overlying tectonic blocks.

Hubert-Ferrari et al. [169] calculated the Colomb stresses for the North Anatolian Fault region. A general direction of these stresses is oriented counterclockwise. Jolivet et al. [180] described the aseismic slip effect within the North Anatolian Fault (NAF) area. This slip is easily explained based on our proposed model of a rotating deep structure affecting the near-surface section.

Civiero et al. [118] constructed horizontal mantle flow field behavior (Figure 12B) for the region under study. The western side of this mantle flow (Figure 12) correlates well with the GPS pattern and satellite-derived gravity isolines caused by the deep mantle structure. Besides this, the mantle flow creates a singular rotating point precisely in the high-magnitude seismogenic zone. Numerous authors have also discovered the counterclockwise rotation of tectonic blocks according to paleomagnetic data [e.g., 10, 22, 57, 61, 65, 67].

The seismotomographic data [117, 118] demonstrate that the shear wave values decreased at the depts 1500-1700 km. This fact indicates the presence of warmed geological rocks coinciding with the upper part of the recognized deep mantle structure. Thus, we can conclude that the mantle structure transfers energy to the above-laying blocks and layers using thermal convection. According to Orovetsky and Kobolev [181], one of the two geodynamic paleo-equatorial nodes of the Earth is located almost in the geometric center of the projection of the identified deep structure.

Trubitsyn's [182] theoretical calculations testify that a 1650–1700 km depth corresponds to the anomalous zone of the spin (phase) transition, which relates to the calculated upper edge of the discovered mantle target. Such zones are the most unstable and often include mantle plumes, which can geodynamically and magmatically affect the upper mantle, crustal blocks, and even characteristics of sedimentary basins (last – in near-surface layers) [2].

A generalization of the seismic tomography anomalies for the northern part of the deep anomalous target was presented in subsection 3.7. Moreover, Kovachev and Krylov [183] directly associate the microseismicity in the eastern part of the lower mantle uplift's projection – the Persian Gulf and the Zagros Mountain Massif – with the revealed counterclockwise rotation of the giant deep structure [16].

5.2. Tectonic-geodynamical and mineralogical-petrological analysis

It was found that the most crucial element of the zone of the junction of the Eurasian and Gondwana platforms is the zone of collision of the Mesozoic terrane belt (MTB) (composed of massifs of thinned continental and oceanic crust) [22] and the Alpine-Himalayan orogenic belt (formed of a highly variegated complex of blocks of continental bark and numerous ophiolites). The most complex section of this junction zone corresponds to the distal protrusion of the MTB,

which intrudes into the Alpine-Himalayan belt in the eastern area of wedging out of the tectonically most complex part of the Anatolian plate (Figures 4 and 11).

Outcrops of different mantle magmatic elements in Eastern Turkey [130, 131, 184], Cyprus [e.g., 129, 130, 185], western-northern Syria [134], Carmel area (northern Israel) [136–140], Makhesh Ramon area (southern Israel) [89, 94, 141], and Central Eastern Desert (Egypt) [143] testify to high tectonic-geodynamic activity in the surface (subsurface) projection of the mantle structure. Obviously, the deep structure's rotation creates, over its projection, particular geodynamic prerequisites for forming mineral deposits.

Lusk et al. [184] investigated the physical-chemical properties of peridotite xenoliths from the North Anatolian fault zone in detail. They concluded that relatively constant differential stress characterizes the lithospheric mantle beneath this area.

The Red Sea rifting zone is part of a deep fault continuing northward to the Carpathian region and intersecting different lithospheric plates and assemblies. This fault coincides with the long axis of the deep mantle structure projection. The deep mantle structure's central (apical) part forms the Sinai Plate and is bounded meridionally by two faults. In the north, the Sinai Plate is bounded by a fault stretching from the southern part of the Aegean–Anatolian Plate. Our data designate the Red Sea's geodynamic asymmetry between the eastern and western coasts [16] caused by the counterclockwise rotation. In the southern part of Cyprus Island, a Cretaceous mantle diapir reaches the surface, and dozens of kilometers south of it, the oldest oceanic crust block relating to the Kiama hyperzone was discovered [21]. The summation of these factors enabled a conclusion on the regularity of the phenomena caused by the influence of the mantle structure.

The structural aspects of the anomalous mantle structure are revealed in plate tectonics, where the linear diagonally oriented Red Sea rift zone with the development of an initial narrow zone of oceanic crust is sharply different from the East African rift zone, and the Gulf of Aden rift.

First of all, it is necessary to pay attention to the fact that the Red Sea rift in the triple junction zone extends almost at a right angle from the hot spot of the Afar triangle (Figure 1) – from the curving line of the rift trough of the Gulf of Aden and East Africa. Such an anomalous structure, which arose as an offshoot in the form of an extended linear marine basin in the distal part of Gondwana, is inexplicable without the presence in this zone of active uplift of the deep mantle with an ascending mantle heat flow. The impact of these phenomena has been widely developed in the Red Sea and described in detail in many publications [e.g., 75].

Mantle plumes could have contributed to the anomalous rifting of the Red Sea in the zone of development of the Precambrian continental crust in the late Cenozoic. However, rifting from this stage could not have manifested itself significantly without the influence of thermal convection from the mantle structure. Regional studies of earlier stages of development of the part of Gondwana prompt this conclusion. A deep magmatic belt was identified here, associated with upwelling mantle flow plumes [84] with the development of the Late Mesozoic Large Igneous Province: basalt traps, deep carbonatite intrusions, kimberlites, lamproites, and diamonds and their deep originated minerals-satellites [134, 136–143]. Structurally, this province is associated with a deep magmatic fault. Its northern part roughly corresponded to the modern Dead Sea Transform zone, and the southern part formed the East Marginal Nubian Fault (EMNF) [22, 186]. These studies indicate the existence of an ancient Mesozoic analog of the axial zone of the deep mantle structure. In the late Cenozoic, it rotated 45° counterclockwise and formed a linearly extended rift zone of the Red Sea.

It is charming to note that several authors [e.g., 187, 188] argue that conventional plate tectonics cannot explain the intraplate (platform) magmatism (traps, flood basalts, kimberlites) and the related metallogeny. Nevertheless, the recognized rotating mantle structure can theoretically explain the origin of linear structures of continental magmatism [16], which remains ineffectually tectonically-geophysically substantiated [187].

The tectonic-structural analysis describes the most significant features of the Earth's crust's regional deformation with a sub-latitudinal Alpine belt and a sub-meridional Neoproterozoic belt with an arcuate protrusion of the MTB in the zone of their junction. The combination of tectonic and paleomagnetic data shows (Figure 1) that deep diagonal faults are developed approximately in this zone, near which the rotation of tectonic blocks in the counterclockwise direction dominates in the west and the east, in the clockwise direction. The zone of catastrophic earthquakes under consideration is developed west of the arcuate ledge.

Figures 1 and 2 indicate that the most active geodynamic processes are developed in the apical part of the deep target contour. In the contact zone of the most active faults (Dead Sea Transform (DST) and Eastern Anatolian Fault (EAF)), deep stresses are discharged in the distal part of the northward-moving Arabian lithospheric plate with the deviation of the focal zones of high-magnitude earthquakes to the south-west, in the direction of counterclockwise block movement (Figure 1). Therefore, the Anatolian plate was shifted in this direction towards the Mediterranean Sea.

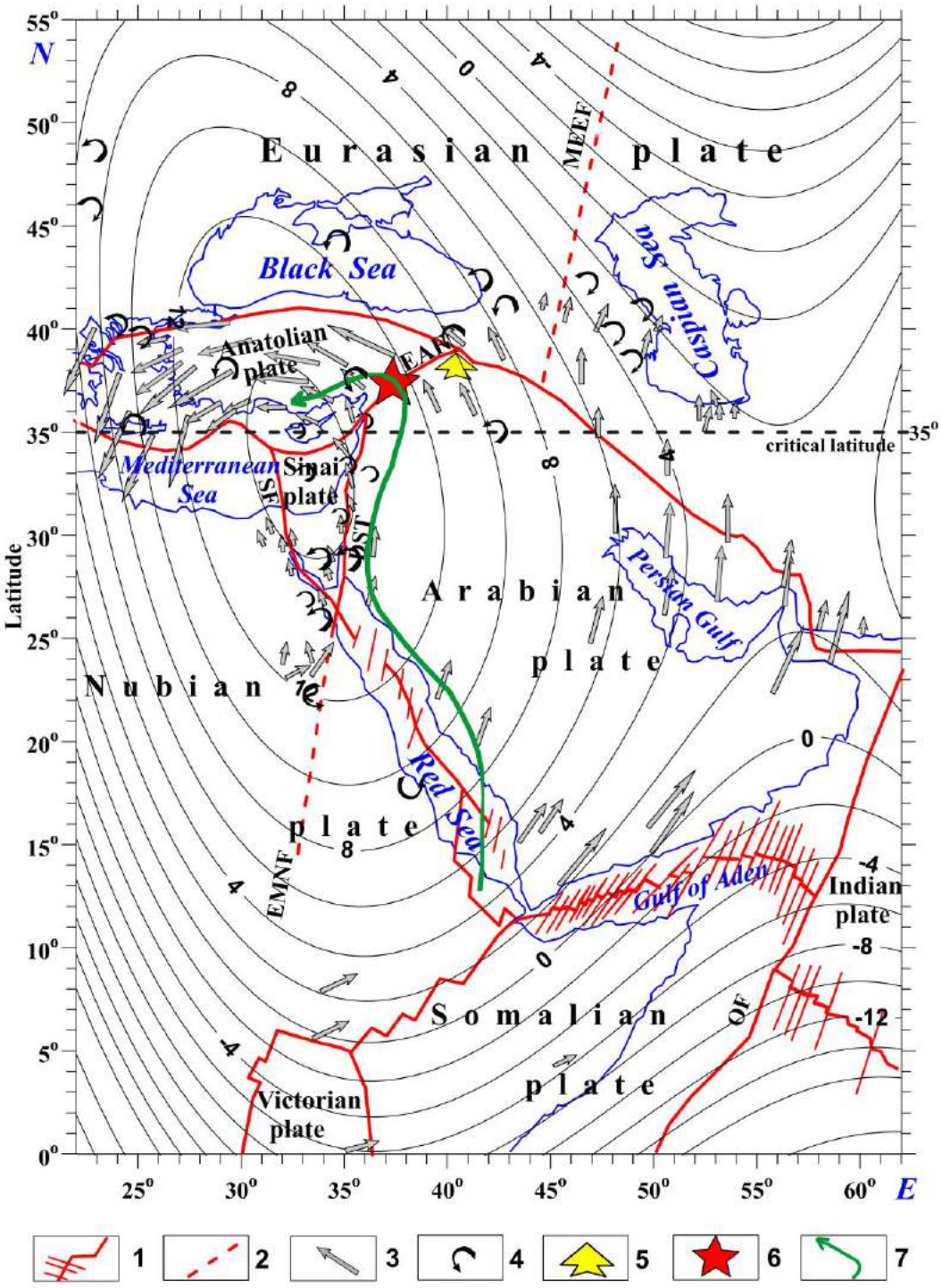

Figure 12. Combined GPS-gravity-paleomagnetic geodynamic scheme with the attraction of horizontal mantle flow direction. (1) main interplate faults, (2) main intraplate faults, (3) vectors of the GPS monitoring (after [14, 29, 30], (4) paleomagnetic vector orientations (observation areas are listed in [16]), (5) distal part of the Mesozoic terrane belt, (6) high magnitude seismogenic zone in Eastern Turkey (02/06/2023), (6) horizontal mantle flow direction (digitized from [118])

5.3. Mathematical analysis

5.3.1. Critical latitude of the Earth

The sublatitudinal critical Earth's latitude of 35° [31] geometrically coincides with the center of deep structure projection [16], which was revealed based on gravity, GPS, paleomagnetic, and magnetic data. It should be noted that the influence of the Earth's rotation was noted in the global seismicity distribution [189]. It is helpful to underline that the Santorini volcano, located near the critical latitude of 35° N and the center of the mantle structure projection, originated one of the most catastrophic events in world history (17th century BCE) [190].

5.3.2. Trivial calculation of the probabilistic criteria

Using trivial mathematical notions, the probability of a random coincidence q of the aforementioned independent indicators is about 1/10,000 (given that we consider only the leading indicators) [e.g., 191]. Accordingly, the probability γ of the existence of the discovered phenomenon ($\gamma = 1 - q$) is vastly high.

5.4. Final summarized factors

The constructed combined physical–geological model verifies the existence of the giant mantle rotating quasi-ring structure and is based on the integration of the following geophysical–geological factors (Table 1).

Table 1. Compiled multidisciplinary phenomena reflecting the existence of huge mantle counterclockwise rotating structure

N	Field / Factor	Explanation	Figure / Reference
1	Satellite gravity	Calculation of the residual gravity anomaly shows the contour of the quasi-circular structure. The results of quantitative interpretation of the residual gravity anomaly indicating its depth	Figure 2
2	Land/marine gravity	Land (marine) gravity anomalies coincide with the satellite-derived residual gravity anomaly	Figure 3
3	Paleomagnetic data analysis	Paleomagnetic data doubtless indicates the predominant counterclockwise rotation of crustal blocks	Figures 1, 6–8
4	GPS pattern	Counterclockwise quasi-circular behavior of the GPS vector distribution	Figure 2; [14, 29, 30, 47]
5	Magnetic data analysis	Circular ΔZ magnetic field pattern at the level of 2.5 km over the mean sea level repeats mainly the residual gravity and GPS designs	Figures 10, 11
6	Geoid isolines' pattern	The geoid's anomalous pattern coinciding with the items (1) and (4)	Figure 5
7	Critical latitude of the Earth	The center of the discovered deep target coincides with the Earth's critical latitude of +35°	Figures 3, 5; [31, 189]
8	Paleobiogeographical data	The paleobiogeographic data analysis indicating the counterclockwise rotation of the surface (near-surface) layers	Figure 9 and sources in captions
9	Asymmetry of sedimentary basins	The geomorphological asymmetry in the Red Sea rift zone, the Dead Sea Basin, and some other areas is mainly geodynamically determined by the counterclockwise rotation	[15, 16, 152]
10	Vast mineralogical- petrological data	The numerous petrological and mineralogical data designating the tectonic and geodynamic activity within the deep mantle projection onto the near-surface part of the geological section	[89, 94, 127, 129, 131, 133–143, 184, 185]
11	Regional seismotomographic studies	The seismotomographic data display the anomalous medium parameters in the lower mantle (~ 1400-1700 km) of the region under study	[112–115, 116–118]
12	Intensive microseismicity of the Persian Gulf and Zagros massif	Kovachev and Krylov (2023) directly associate the microseismicity in this region (up to 180 km deep) with the rotating mantle structure (initially revealed in Eppelbaum et al. (2021)). The deep anomalous zones in this region were detected by Civiero et al. (2023)	[118, 183]
13	Oceanic crust block relating to the Kiama paleomagnetic hyperzone	The crucial impact of the deep structure just prevented the oceanic block subduction and conserved its location till the present	Figures 1, 5, 10, 11; [21, 22, 144]
14	Numerous tectonic-geodynamic data	First, the results of the last catastrophic earthquakes in Eastern Turkey, when the large land segments were displaced counterclockwise	Figures 1, 2, 4; [7, 161, 172–174]
15	Uplift of the upper surface of the contrast density surface in the lithosphere	The uplifted part of the contrast density surface computed using 3D inverse methods coincides with the long axis of the deep mantle structure	[13]
16	Horizontal mantle flow direction	The horizontal mantle flow direction correlates well with the GPS data and gravity isoline pattern. Besides this, the flow has a singular rotation point directly in the area of the Turkish earthquakes of 06.02.2023	Figure 12; [118]

5.5. A few factors reflecting the mantle nature of the discovered geodynamic phenomenon

We want to pay special attention to the mantle origin of the revealed integrated regional geological-geophysical phenomenon. The determined factors are collected in one subsection for the convenience of readers:

(1) The quantitative analysis of the residual satellite-derived gravity anomaly gave a depth of 1650-1700 km,
(2) The geoid isolines map (like the gravity residual map) undoubtedly indicates the deep origin of the target occurrence,

(3) The critical latitude of the Earth (35°) effect is the global geodynamic factor and cannot be connected in any way with the near-surface (in our case, tens of km) structures,
(4) The seismotomographic studies show some anomalous zones at a depth of 1,400-1,700 km in the studied region,
(5) The numerous mineralogical-petrological data imply the presence of an anomalous volume of minerals and rocks of the mantle origin,
(6) Comprehensive analysis of physical-chemical properties of peridotite xenoliths [184] indicates constant differential stress in the mantle lithosphere below the North Anatolian Fault zone within the deep structure projection.

6. Conclusions

This geodynamic phenomenon's mantle (deep) origin follows from several of the evidence presented. The multi-method study highlights the relationship between the revealed counterclockwise rotating mantle structure and different subsurface geological-geophysical features. The probabilistic estimate of a random coincidence of all these factors (satellite and surface gravity, GPS vector distribution, airborne magnetic field pattern, paleomagnetic vector orientation, geoid isoline pattern, Earth's critical latitude, paleobiogeographical constructions, asymmetry of sedimentary basins, seismotomographic data, mineralogical- petrological analysis, oceanic crust block relating to the Kiama paleomagnetic hyperzone, and numerous tectonic-structural data), is extremely small. We believe that this structure influenced the origin of the Cyprus high-amplitude gravity anomaly, the Sinai Plate configuration, the counterclockwise rotation of the Mesozoic terrane belt, the geometry of asymmetric basins along the Dead Sea Transform, and the displacement of the tectonic block corresponding to the Kiama paleomagnetic hyperzone in the Eastern Mediterranean. The discovery of a deep anomalous structure explains the existence of intraplatform magmatic belts that had not previously found explanations within the framework of existing theories. The rotating mantle ring structure, influencing many tectonic–geodynamic processes, maybe a global geodynamic factor contributing to the spreading of the Red Sea. We propose that the giant accumulated stress caused by the deep mantle structure's counterclockwise rotation was the significant reason (joined with the known dangerous seismological faulting in this area) that caused the catastrophic Turkish earthquakes on February 06, 2023. Further investigation of this phenomenon should include mutual geophysical-geological studies to reveal zones with the most stress accumulation and high seismic activity.

Authors Contribution

Lev Eppelbaum: main idea, review of literature, comparison of different concepts, integrating physical-geological methods, tectonic-geodynamic conclusions, development of maps

Youri Katz: review of literature, comparison of different concepts, integrating physical-geological methods, tectonic-geodynamic conclusions, development of maps

Zvi Ben-Avraham: review of literature, comparison of different concepts, integrating physical-geological methods, tectonic-geodynamic conclusions, development of maps

References

[1] Allen, P. A., 2011. Surface impact of mantle processes. *Nature Geosciences*, 498-499. https://doi.org/10.1038/ngeo1216

[2] Trubitsyn, V. P., 2012. Propagation of oceanic plates through the boundary between the upper and lower mantle. *Doklady Earth Sci*., **446**, 1220-1222. https://doi.org/10.1134/S1069351308030014

[3] Cloetingh, S., Willet, S. D., 2013. Linking deep Earth and surface processes. *EOS*, Trans. Am. Geophys. Union, **94**, 53-54. https://doi.org/10.1002/2013EO050002

[4] Domeier, M., Doubrovine, P. V., Torsvik, T. H., Spakman, W., Bull, A. L., 2016. Global correlation of lower mantle structure and past subduction. *Geophysical Research Lett.*, **43**, 4945-4953. https://doi.org/10.1002/2016GL068827

[5] Cloetingh, S., Tibaldi, A., Dobrzhinetskaya, L., Matenco, L., Nader, F. and de Vries, B. v. W., 2018. From the deep Earth to the surface: A multiscale approach. *Global Planet. Change*, **171**, 1-322.

[6] Marquardt, H., Ballmer, M., Cottaar, S. and Konter, J. (Eds.), 2021. *Mantle Convection and Surface Expressions*. Amer. Geophysical Union, Geoph. Monograph Series, Wiley, N.J., USA, 512 p.

[7] Karabulut, H., Güvercin, S.E., Hollingsworth, J. and Konca1, A.Ö., 2023. Long silence on the East Anatolian Fault Zone (Southern Turkey) ends with devastating double earthquakes (6 February 2023) over a seismic gap: implications for the seismic potential in the Eastern Mediterranean region. *Jour. of the Geological Society*, London, **180**, 1-10. https://doi.org/10.1144/jgs2023-021

[8] Ben-Avraham, Z., Ginzburg, A., Makris, J. and Eppelbaum, L., 2002. Crustal structure of the Levant basin, eastern Mediterranean. *Tectonophysics*, **346**, 23-43. https://doi.org/10.1016/S0040-1951(01)00226-8

[9] Ben-Avraham, Z., Schattner, U., Lazar, M., Hall, J.K., Ben-Gai, Y., Neev, D. and Reshef, M., 2006. Segmentation of the Levant continental margin, eastern Mediterranean. *Tectonics*, **25**, TC5002, 1-17. https://doi.org/10.1029/2005TC00182426

[10] Tatar, O., Piper, J.D.A., Gürsoy, H., Heimann, A. and Koşbulut, F., 2004. Neotectonic deformation in the transition zone between the Dead Sea Transform and the East Anatolian Fault Zone, Southern Turkey: a palaeomagnetic study of the Karasu Rift Volcanism. *Tectonophysics*, **385**, 17-43. https://doi.org/10.1016/j.tecto.2004.04.005

[11] Faccenna, C., Becker, T.W., Auer, L., Billi, A., Boschi, L., Brun, J.P., Capitanio, F.A., Funiciello, F., Horvàth, F., Jolivet, L., Piromallo, C., Royden, L., Rossetti, F. and Serpelloni, E., 2014. Mantle dynamics in the Mediterranean. *Review of Geophysics*, **52**, 283–332. https://doi.org/10.1002/2013RG000444

[12] Uzel, B., Langereis, C. G., Kaymakci, N., Sozbilir, H., Ozkaymak, C. and Ozkaptan, M., 2015. Paleomagnetic Evidence for an Inverse Rotation History of Western Anatolia during the Exhumation of Menderes Core Complex. *Earth and Planet. Sci. Lett*., **414**, 108-125. https://doi.org/10.1016/j.epsl.2015.01.008

[13] Eppelbaum, L**.**, Katz, Yu., Klokochnik, J., Kosteletsky, J., Zheludev, V. and Ben-Avraham, Z., 2018. Tectonic Insights into the Arabian-African Region Inferred from a Comprehensive Examination of Satellite Gravity Big Data. *Global and Planetary Change*, **171**, 65–87. https://doi.org/10.1016/j.gloplacha.2017.10.011

[14] Reilinger, R. E., McClusky, S., Vernant, P., Lawrence, S., Ergintav, S., Cakmak, R., Ozener, H., Kadirov, F., Guliyev, I. et al., 2006. GPS constraints on continental deformation in the Africa-Arabia-Eurasia continental collision zone and implications for the dynamics of plate interactions. *Jour. of Geophysical Research*, **BO5411**, 1–26. https://doi.org/10.1029/2005JB004051

[15] Eppelbaum, L. V., Ben-Avraham, Z., Katz, Y., Cloetingh, S., Kaban, M., 2020. Combined Multifactor Evidence of a Giant Lower-Mantle Ring Structure Below the Eastern Mediterranean. *Positioning*, **11**, 11–32. https://doi.org/10.4236/pos.2020.112002

[16] Eppelbaum, L. V., Ben-Avraham, Z., Katz, Y., Cloetingh, S., Kaban, M., 2021. Giant quasi-ring mantle structure in the African-Arabian junction: Results derived from the geological-geophysical data integration. *Geotectonics* (Springer), **55**, No. 1, 67–93. https://doi.org/10.1134/S0016852121010052

[17] Ambraseys, N.N. and Finkel, C.F., 1995. *Seismicity of Turkey and adjacent areas: a historical review, 1500–1800*. Eren Yayinlari Publ., 240 p.

[18] Alpyürür, M. and Lav, M.A., 2022. An assessment of probabilistic seismic hazard for the cities in Southwest Turkey using historical and instrumental earthquake catalogs. *Natural Hazards*, **114**, 335-365. https://doi.org/10.1007/s11069-022-05392-x

[19] Wells, D.L. and Coppersmith, K.J., 1994. New empirical relationships among magnitude, rupture length, rupture width, rupture area and surface displacement. *Bull. of the Seismol. Society of America*, 84(4), 974-1002. https://doi.org/10.1785/BSSA0840040974

[20] Khesin, B.E., Alexeyev, V.V. and Eppelbaum, L.V., 1996. *Interpretation of Geophysical Fields in Complicated Environments*. Modern Appr. in Geophysics, Vol. **14**, Kluwer, Dordrecht, 368 p.

[21] Eppelbaum, L.V., Nikolaev, A.V. and Katz, Y.I., 2014. Space location of the Kiama paleomagnetic hyperzone of inverse polarity in the crust of the eastern Mediterranean. *Doklady Earth Sciences* (Springer), **457**, No. 6, 710-714. https://doi.org/10.1134/S1028334X14080212

[22] Eppelbaum, L.V. and Katz, Yu.I., 2015. Eastern Mediterranean: Combined geological-geophysical zonation and paleogeodynamics of the Mesozoic and Cenozoic structural-sedimentation stages. *Marine and Petroleum Geology*, **65**, 198–216. https://doi.org/10.1016/j.marpetgeo.2015.04.008

[23] Faccenna, C., Jolivet, L., Piromallo, C. and A. Morelli, 2003. Subduction and depth of convection in the Mediterranean mantle. *Jour. of Geophys. Res*.: Solid Earth, **108**, 1-13. https://doi.org/10.1029/2001JB001690

[24] Muttoni, G., Kent, D.V., Garzanti, E., Brack, P., Abrahamsen, N. and Gaetani, M., 2003. Early Permian Pangea 'B' to Late Permian Pangea 'A'. *Earth Planet. Sci. Lett*., **215**, 379-394. https://doi.org/10.1016/S0012-821X(03)00452-7

[25] Stampfli, G.M., Hochard, C., Verard, C., Wilhem, C. and von Raumer, J., 2013. The formation of Pangea. *Tectonophysics*, **593**, 1-19. https://doi.org/10.1016/j.tecto.2013.02.037

[26] Rolland, Y., Hassig, M., Bosch, D., Bruguier, D., Melis, R., Galoyan, G., Topuz, G., Sahakyan, L., Avagyan, A. and Sosson, M., 2020. The East Anatolia–Lesser Caucasus ophiolite: An exceptional case of large-scale obduction, synthesis of data and numerical modelling. *Geosci. Front*., **11**, 83-108. https://doi.org/10.1016/j.gsf.2018.12.009

[27] Stern, R.J. and Johnson, P.R., 2010. Continental lithosphere of the Arabian Plate: A geologic, petrologic, and geophysical synthesis. *Earth-Sci. Rev*., **101**, 29-67. https://doi.org/10.1016/j.earscirev.2010.01.002

[28] Jolivet, L., Faccenna, L., Agard, P., de Lamotte, D. F., Menant, A., Sternai, P. and Guillocheau, F., 2016. Neo-Tethys geodynamics and mantle convection: From extension to compression in Africa and a conceptual model for obduction. *Canad. J. Earth Sci*., **53**, 1-15. https://doi.org/10.1139/cjes-2015-0118

[29] Mahmoud, S.M., 2003. Seismicity and GPS-derived crustal deformation in Egypt. *Geodynamics*, **35**, 333-352. https://doi.org/10.1016/S0264-3707(02)00135-7

[30] Khaffou, M., Raji, M. and El-Ayachi, M., 2023. East African Rift Dynamics. *E3S Web of Conferences*, 412, 01030, 1-10. https://doi.org/10.1051/e3sconf/202341201030

[31] Véronnet, A., 1912. Rotation de l'Ellipsoide Hétérogène et Figure Exacte de la Terre. *J. Math. Pures et Appl*., **8**, Ser. 6, 331–463.

[32] Barka, A. and Reilinger, R., 1997. Active tectonics of the Eastern Mediterranean region: deduced from GPS, neotectonic, and seismicity data. *Ann. Geophys*., **40**, 587-610.

[33] McClusky, S. et al., 2000. Global Positioning System constraints on plate kinematics and dynamics in the eastern Mediterranean and Caucasus. *Jour. of Geophys. Res*., **105**, 5695-5719. https://doi.org/10.1029/1999JB900351

[34] Boschi, L., Faccenna, C. and Becker, T.W., 2010. Mantle structure and dynamic topography in the Mediterranean basin. *Geophys. Res. Lett*., **37**, L20303, 1-5. https://doi.org/10.1029/2010GL045001

[35] Eppelbaum, L.V. and Katz, Y.I., 2012b. Key features of seismo-neotectonic pattern of the Eastern Mediterranean. *Izvestiya, Acad. Sci. Azerb. Rep*., Ser.: Earth Sci., No. 3, 29-40.

[36] Eppelbaum, L.V. and Katz, Yu.I., 2017. A New Regard on the Tectonic Map of the Arabian-African Region Inferred from the Satellite Gravity Analysis. *Acta Geophysica*, **65**, 607-626. https://doi.org/10.1007/s11600-017-0057-2

[37] Eppelbaum, L. and Katz, Yu., 2020. Significant tectonic-geophysical features of the African-Arabian tectonic region: An overview. *Geotectonics* (Springer), **54,** No. 2, 266-283. https://doi.org/10.1134/S0016852120020041

[38] Kaban, M.K., El Khrepy, S., Al-Arifi, N., Tesauro, M. and Stolk, W., 2016. Three-dimensional density model of the upper mantle in the Middle East: Interaction of diverse tectonic processes. *Jour. of Geophys. Res.*, Ser.: Solid Earth, **121**, 5349-5364. https://doi.org/10.1002/2015JB012755

[39] Sandwell, D.T. and Smith, W.H.F., 2009. Global marine gravity from retracked Geosat and ERS-1 altimetry: ridge segmentation versus spreading rate. *Jour. of Geophysical Research*, 114(B01411), 1–18. https://doi.org/10.1029/2008JB006008

[40] Barbeau, E.J., 2003. *Polynomials*. Springer, New York, 455 p.

[41] Telford, W.M., Geldart, L.R. and Sheriff, R.E., 2004. *Applied Geophysics*. Cambridge Univ. Press (2nd ed.), Cambridge, 770 p.

[42] Eppelbaum, L.V. and Khesin, B.E., 2012. *Geophysical Studies in the Caucasus*. Springer, Heidelberg, 411 p.

[43] Aleinikov, A.L., Belikov, V.T. and Eppelbaum, L.V., 2001. Some Physical Foundations of Geodynamics (in Russian, contents, and summary in English). *Kedem Printing-House*, Tel Aviv, Israel, 172 p.

[44] Makris, J., Henke, C.H., Egloff, F. and Akamaluk, T., 1991. The gravity field of the Red Sea and East Africa. *Tectonophysics*, **198**, 369-381. https://doi.org/10.1016/0040-1951(91)90161-K

[45] Gass, I.G. and Masson-Smith, D., 1963. The geology and gravity anomalies of the Troodos Massif, Cyprus. *Philos. Trans. R. Soc*. London, Ser. A **255**, 417-466. https://doi.org/10.1098/rsta.1963.0009

[46] Garini, E. and Gazeras, G., 2023. The 2 earthquakes of February 6th, 2023, in Turkey. Preliminary Report. NTUA, Greece.

[47] Doubre, C., Deprez, A., Masson, F., Socquet, A., Lewi, E., Grandin, R., Nercessian, A., Ulrich, P., De Chabalier, J.-B., Saad, I., Abayazid, A., Peltzer, G., Delorme, A., Calasis, E. and Wright, T., 2017. Current deformation in Central Afar and triple junction kinematics deduced from GPS and InSAR measurements. *Geophys. Jour. Intern*., **208,** 936-953. https://doi.org/10.1093/gji/ggw434

[48] Richards, M.A. and Hager, B.H., 1984. Geoid anomalies in a dynamic Earth. *Jour. of Geophysical Research*, **B 89**, 5987–6002. https://doi.org/10.1029/JB089iB07p05987

[49] Ricard, Y., Vigny, C. and Froidevaux, C., 1989. Mantle heterogeneities, geoid, and plate motion: a Monte Carlo inversion. *Jour. of Geophysical Research*, **94** (B10), 13,739-13,754. https://doi.org/10.1029/JB094iB10p13739

[50] Mao, W. and Zhong, S., 2021. Constraints on mantle viscosity from intermediate-wavelength geoid anomalies in mantle convection models with plate motion history. *Jour. of Geoph. Research*: Solid Earth, **126**, e2020JB021561, 1-25. https://doi.org/10.1029/2020JB021561

[51] National Geospatial-Intelligence Agency, EGM2008 – WGS 84 Version. https://earth-info.nga.mil/GandG/wgs84/gravitymod/egm2008/egm08_wgs84.html. Accessed December 12, 2023.

[52] Kissel, C. and Laj, C., 1988. *Paleomagnetic Rotations and Continental Deformation*. NATO ASI Series: Mathematical and Physical Sciences. Kluwer Academic Publishers: Dordrecht, The Netherlands; Boston, USA; London, UK, 530 p.

[53] McElhinny, M.W., 1989. *Paleomagnetism and Plate Tectonics*. Cambridge Univ. Press, 235 p.

[54] Tauxe, L., 2002. *Paleomagnetic Principles and Practice*. Kluwer Acad. Publishers, N.Y. – Boston – Dordrecht, 299 p.

[55] Khramov, A.N., 1984. *Paleomagnetic Directions and Pole Positions: Data for the USSR (Catalogue)*, No. 1 of *World Data Center, Ser. B*, Geophys. Comm. Acad. Sci. SSSR, Moscow.

[56] Nur, A., Ron, H. and Scott, O., 1989. Mechanics of distributed fault and block rotation. In: (C. Kissel and C. Laj, Eds.), *Paleomagnetic Rotations and Continental Deformation*, Kluwer Academic Publ., 209-228. https://doi.org/10.1007/978-94-009-0869-7_14

[57] Platzman, E.S., Platt, J.P., Tapirdamaz, C., Sanver, M. and Rundle, C.C., 1994. Why are there no clockwise rotations along the North Anatolian Fault Zone? Journal of Geophysical Research: Solid Earth, **99**(B11), 21705–21715. https://doi.org/10.1029/94JB01665

[58] Duermeijer, C.E., Krijgsman, C.E., Langereis, C.G. and Ten Veen, J.H., 1998. Post-early Messinian counterclockwise rotations on Crete: Implications for Late Miocene to recent kinematics of the southern Hellenic arc. *Tectonophysics*, **298**, 177-189. https://doi.org/10.1016/S0040-1951(98)00183-8

[59] Kissel, C., Laj, C., Poisson, A. and Gorur, N., 2003. Paleomagnetic reconstruction of the Cenozoic evolution of the Eastern Mediterranean. *Tectonophysics*, **362**, 199-217. https://doi.org/10.1016/S0040-1951(02)00638-8

[60] Marchev, P., Raicheva, R., Downes, H., Vaselli, O., Chiaradia, M. and Moritz, R., 2004. Compositional diversity of Eocene–Oligocene basaltic magmatism in the Eastern Rhodopes, SE Bulgaria: Implications for genesis and tectonic setting. *Tectonophysics*, **393**, 301-328. https://doi.org/10.1016/j.tecto.2004.07.045

[61] Piper, J.D.A., Tatar, O., Gürsoy, H., Koçbulut, F. and Mesci, B.L., 2006. Paleomagnetic analysis of neotectonic deformation in the Anatolian accretionary collage, Turkey. In: (Dilek, Y. and Pavlides, S., Eds.), *Postcollisional Tectonics and Magmatism in the Mediterranean Region and Asia*. Geol. Soc. of America Spec. Paper **409**, 417-439. https://doi.org/10.1130/2006.2409(20)

[62] Borradaile, G.J., Lagroix, F., Hamilton, T.D. and Trebilcock, D.A., 2010. Ophiolite tectonics, rock magnetism and paleomagnetism, Cyprus. *Surv. Geophys*., **31**, 285-359. https://doi.org/10.1007/s10712-009-9090-2

[63] Henry, B., Homberg, C., Mroueh, M., Hamdan, W. and Higazi, W., 2010. Rotations in Lebanon inferred from new palaeomagnetic data and implications for the evolution of the Dead Sea Transform system. In (C. Homberg and M. Bachman, Eds.), *Evolution of the Levant Margin and Western Arabia Platform since the Mesozoic*, Vol. 341 of Geol. Soc. London, Spec. Publ., 269-285. https://doi.org/10.1144/SP341.13

[64] Lotfi, H.I., 2015. Early Cretaceous counterclockwise rotation of Northeast Africa within the equatorial zone: Paleomagnetic study on Mansouri ring complex, Southeastern Desert, Egypt. *NRIAG J. Astron. Geophys*., **4**(1), 1-15.

[65] Gürer, D., van Hinsbergen, D.J.J., Özkaptan, M., Creton, I., Koymans, M.R., Cascella, A. and Langereis, C.G., 2017. Paleomagnetic constraints on the timing and distribution of Cenozoic rotations in Central and Eastern Anatolia. *Solid Earth Discuss*., https://doi.org/10.5194/se-2017-66

[66] Çabuk, B.S. and Cengiz, M., 2021. Paleomagnetic rotations in the circum-Marmara region, northwestern Turkey since the Late Cretaceous. *Jour. of Asian Earth Sci*., **213**, 104748, 1-15. https://doi.org/10.1016/j.jseaes.2021.104748

[67] Lazos, I., Sboras, S., Chousianitis, K., Kondopoulou, D., Pikridas, C., Bitharis, S. and Pavlides, S., 2022. Temporal evolution of crustal rotation in the Aegean region based on primary geodetically-derived results and palaeomagnetism. *Acta Geodaetica et Geophysica*, **57**,317–334. https://doi.org/10.1007/s40328-022-00379-3

[68] Bazhenov, M.L. and Burtman, V.S., 2002. Eocene paleomagnetism of the Caucasus (southwest Georgia): Oroclinal bending in the Arabian syntaxis. *Tectonophysics*, **344**, 247-259. https://doi.org/10.1016/S0040-1951(01)00189-5

[69] Hisarli, Z.Z.M., 2011. New paleomagnetic constraints on the Late Cretaceous and Early Cenozoic tectonic history of the Eastern Pontides. *Jour. of Geodynamics*, **52**, 114–128. https://doi.org/10.1016/j.jog.2010.12.004

[70] Rolland, Y., 2017. Caucasus collisional history: Review of data from East Anatolia to West Iran. *Gondwana Research*, **49**, 130-146. https://doi.org/10.1016/j.gr.2017.05.005

[71] Khalafly, A.A., 2006. *Paleomagnetism of the Lesser Caucasus*. Takhsil, Baku, 189 p. (in Russian).

[72] Molostovsky, E.A., Pechersky, D.M. and Frolov, I.Yu., 2007. Magnetostratigraphic Timescale of the Phanerozoic and Its Description Using a Cumulative Distribution Function. *Izvestiya, Physics of the Solid Earth*, **43**(10), 811–818. https://doi.org/10.1134/S1069351307100035

[73] Pechersky, D.M., Lyubushin, A.A. and Sharonova, Z.V., 2010. On the synchronism in the events within the core and on the surface of the earth: the changes in the organic world and in the polarity of the geomagnetic field in the Phanerozoic. *Izvestiya, Physics of the Solid Earth*, **46**, 613-623. https://doi.org/10.1134/S1069351310070050

[74] Morris, A., Erson, M.W., Robertson, A.H. and Al-Riyami, K., 2002. Extreme tectonic rotations within an eastern Mediterranean ophiolite (Baer–Bassit, Syria). *Earth Planet. Sci. Lett*., **202**, 247-261. https://doi.org/10.1016/S0012-821X(02)00782-3

[75] Hall, J.K., Krasheninnikov, V.A., Hirsch, F., Benjamini, C. and Flexer, A., 2005. *Geological Framework of the Levant*, Vol. 2: *The Levantine Basin and Israel*. Historical Productions-Hall, Jerusalem, Israel.

[76] Sneh, A., Bartov, Y. and Rozensaft, M., 1998. Geological Map of Israel, Scale 1:200,000. *Geol. Surv. of Israel*, Min. of Nation. Infrastructure, Jerusalem.

[77] Lang, B. and Steinitz, G., 1989. K-Ar dating of Mesozoic magmatic rocks in Israel: A review. *Isr. Jour. of Earth Sci*., **38**, 89-103.

[78] Eppelbaum, L.V. and Katz, Y.I., 2022. Paleomagnetic-geodynamic mapping of the transition zone from ocean to the continent: A review. *Applied Sciences*, **12**, Spec. Issue: ***Advances in Applied Geophysics***, 1-20. https://doi.org/10.3390/app12115419

[79] Baer, G., Heimann, A., Eshet, Y., Weinberger, R., Mussett, A. and Sherwood, G., 1995. The Saharonim Basalt: A Late Triassic – Early Jurassic intrusion in southeastern Makhtesh Ramon, Israel. *Israel Jour. of Earth Sci*., **44**, 1-10.

[80] Garfunkel, Z. and Katz, A., 1967. New magmatic features in Makhtesh Ramon, southern Israel. *Geological Magazine*, **104** (No. 6), 608-629. https://doi.org/10.1017/S0016756800050275

[81] Zak, I., 1968. Geological Map of Israel (1:20,000). Makhtesh Ramon, Har Gevanim. Israel Geol. Survey.

[82] Baer, G. and Reches, Z., 1991. Mechanics of emplacement and tectonic implications of the Ramon dike systems, Israel. *Jour. of Geophysical Research*, **96**(B7), 11895-11910. https://doi.org/10.1029/91JB00371

[83] Baer, G., 1993. Flow directions in sills and dikes and formation of cauldrons in eastern Makhtesh Ramon. *Israel Jour. of Earth Sci*., **42**, 133-148.

[84] Segev, A., 2000. Synchronous magmatic cycles during the fragmentation of Gondwana: Radiometric ages from the Levant and other provinces. *Tectonophysics*, **325**(3-4), 257-277. https://doi.org/10.1016/S0040-1951(00)00122-0

[85] Avni, Y., 2001. Har Loz, Sheet 21-III. Geological Map of Israel 1:50,000, *Geol. Survey of Israel*, Jerusalem.

[86] Zilberman, E. and Avni, Y., 2004a. The geological map of Israel, 1:50,000. Sheet 21-I, Har Hamran. Israel Geol. Surv., Jerusalem.

[87] Zilberman, E. and Avni, Y., 2004b. The geological map of Israel, 1: 50,000. Sheet 21-II: Mizpe Ramon. Israel Geol. Surv., Jerusalem.

[88] Segev, A., Weissbrod, T. and Lang, B., 2005. $^{40}Ar/^{39}Ar$ dating of the Aptian-Albian igneous rocks in Makhtesh Ramon (Negev, Israel) and its stratigraphic implications. *Cretaceous Research*, **26**, 633-656. https://doi.org/10.1016/j.cretres.2005.03.003

[89] Vapnik, Y., Sharygin, V., Samoilov, V. and Yudalevich, Z., 2007. The petrogenesis of basic and ultrabasic alkaline rocks of Western Makhtesh Ramon, Israel: melt and fluid inclusion study. *Int. Jour. Earth Sci.* (Geol. Rundsh.), **96**, 663-684. https://doi.org/10.1007/s00531-006-0131-5

[90] Yudalevich, Z.A., Fershtater, G.B. and Eyal, M., 2014. Magmatism of Makhtesh-Ramon: Geology, geochemistry, petrogenesis (Conservation area Har Ha-Negev, Israel). *Lithosphere*, No. 3, 70-92 (in Russian).

[91] Avni, Y., Bartov, Y. and Shen, A., 2016. Har Ardon, Sheet 22-I. Geological Map of Israel 1:50,000, *Geol. Survey of Israel*, Jerusalem.

[92] Avni, Y., Beker, A. and Zilberman, E., 2017. Be'erot Oded, Sheet 21-IV. Geological Map of Israel 1:50,000, *Geol. Survey of Israel*, Jerusalem.

[93] Baer, Y., Soudry, D., Bar, O. and Shen, A., 2017. Zofar, Sheet 22-III, IV. Geological Map of Israel 1:50,000, *Geol. Survey of Israel*, Jerusalem.

[94] Yudalevich, Z. and Vapnik, E., 2018. Xenocrysts and megacrysts of alkali-olivine-basalt-basanite-nephelinite association of Makhtesh Ramon (Israel): Interaction with transporting magmas and morphological adjustment. *Lithosphere*, **18**, No. 5, 70-92 (in Russian).

[95] Ron, H. and Baer, G., 1988. Paleomagnetism of Early Cretaceous rocks from southern Israel. *Israel Jour. of Earth Sci.*, **37**, 73-81.

[96] Gvirtzman, G., Weissbrod, T., Baer, G. and Brenner, J., 1996. The age of Aptian stage and its magmatic events: New Ar-Ar ages and paleomagnetic data from the Negev, Israel. *Cretaceous Research*, **17**, 293-310. https://doi.org/10.1006/CRES.1996.0021

[97] Eppelbaum, L.V., Katz, Y.I. and Ben-Avraham, Z., 2012. Israel – Petroleum Geology and Prospective Provinces. *AAPG European Newsletter*, No. 4, 4-9.

[98] Shimron, A.E. and Lang, B., 1989. New geological data and K-Ar geochronology of the magmatic rocks on the southeast flanks of Mount Hermon. *Geol. Surv. Israel Rep.* GSI/41/88.

[99] Wilson, M., Shimron, A.E., Rosenbaum, J.M., Preston, J., 2000. Early Cretaceous magmatism of Mount Hermon, Northern Israel. *Contrib. to Mineralogy and Petrology*, **139**, No. 1, 54-67. https://doi.org/10.1007/s004100050573

[100] Shimron, A.E. and Peltz, S., 1993. Early Cretaceous pyroclastic volcanism on the Hermon Range. *Geol. Surv. Israel Bull*., **84**, p. 43.

[101] Lang, B. and Shimron, A.E., 1991. New K-Ar data of the Mount Hermon Mesozoic magmatic rocks. *Ministry of Energy and Infrastructure*, Geol. Surv. Israel, *Min. Energy Resources Division*, Report GSI/26/91.

[102] Frank, U., Schwab, M.J. and Negendank, J.F.W., 2002. A lacustrine record of paleomagnetic secular variations from Birkat Ram, Golan Heights (Israel) for the last 4400 years. *Phys. Earth Planet. Inter*., **133**, 21-34. https://doi.org/10.1016/S0031-9201(02)00085-7

[103] Segev, A. and Lang, B., 2002. 40Ar/39Ar dating of Valanginian top Tayasir Volcanics in the Mount Hermon area, northern Israel. Israel Geological Survey, *Current Research*, **13**, 100-104.

[104] Behar, G., Shaar, R., Tauxe, L., Asefaw, H., Ebert, Y., Heimann, A., Koppers, A.A.P. and Ron, H., 2019. Paleomagnetism and paleosecular variations from the Plio-Pleistocene Golan Heights volcanic plateau, Israel. *Geochemistry, Geophysics, Geosystems*, 4319-4334. https://doi.org/10.1029/2019GC008479

[105] Lang, B. and Mimran, Y., 1985. An Early Cretaceous volcanic sequence in central Israel and its significance to the absolute date of the base of the Cretaceous. *J. of Geology*, **93**, 179-184. https://doi.org/10.1086/628939.
[106] Mor, D., Mihelson, H., Druckman, Y., Mimran, Y., Heimann, A., Goldberg, M. and Sneh, A., 1997. Notes on the geology of Golan Heights. *Report GSI/15/97*, Jerusalem, 1-18.
[107] Shimron, A.E., 1998. Tectonic evolution of the southern Mount Hermon. *Report Geol. Surv. Israel Rep*. GSI/10/98.
[108] Segev, A., 2009. $^{40}Ar/^{39}Ar$ and K-Ar geochronology of Berriasian-Hauteririan and Cenomanian tectomagmatic events in northern Israel: implications for regional stratigraphy. *Cretaceous Research*, **30**, 818-828. https://doi.org/10.1016/j.cretres.2009.01.003
[109] Segev, A. and Sass, E., 2009. The geology of the Carmel region, Albian-Turonian volcano-sedimentary cycles on the northwestern edge of the Arabian platform. *Rep. of the Israel Geol. Soc*., Jerusalem, 1-77.
[110] Andersson, D.L., 2007. *New Theory of the Earth*, 2nd ed. Cambridge Univ. Press, Cambridge, 400 p.
[111] Khain, V.E. and Koronovskii, N.V., 2007. *Planet Earth: From the Core to The Ionosphere*. Moscow. State. Univ., Moscow (in Russian).
[112] Su, W.-J., Woodward, R.L. and Dziewonski, A.M., 1994. Degree-12 model of shear velocity heterogeneity in the mantle. *Jour. of Geophys. Research*, Solid Earth, **99**, 4945-4980. https://doi.org/10.1029/93JB03408
[113] van der Hilst, R.D., Widiyantoro, S. and Engdahl, E.R., 1997. Evidence for deep mantle circulation from global tomography. *Nature*, **386**, 578-584. https://doi.org/10.1038/386578a0
[114] Wen, L. and Helmberger, D.V., 1998. Ultra-low velocity zones near the core-mantle boundary from broadband PKP precursors. *Science*, **279**, 1701-1703. https://doi.org/10.1126/science.279.5357.17
[115] Schmid, C., van der Lee, S., VanDecar, J.C., Engdahl, E.R. and Giardini, D., 2008. Three-dimensional S velocity of the mantle in the Africa-Eurasia plate boundary region from phase arrival times and regional waveforms. *Jour. of Geophys. Research*: Solid Earth **113**, Art. No. B03306. https://doi.org/10.1029/2005JB004193
[116] Shephard, G.E., Matthews, K.J., Hosseini, K. and Domeier, M., 2017. On the consistency of seismically imaged lower mantle slabs. *Scientific Reports*, **7**, 10976, 1-17. https://doi.org/10.1038/s41598-017-11039-w
[117] van der Meer, D.G., van Hinsbergen, D.J.J. and Spakman, W., 2018. Atlas of the underworld: Slab remnants in the mantle, their sinking history, and a new outlook on lower mantle viscosity. *Tectonophysics*, **723**, 309-448. https://doi.org/10.1016/j.tecto.2017.10.004
[118] Civiero, C., Celli, N.K. and Tesauro, M., 2023. Revisiting the geodynamics of the Middle East region from an integrated geophysical perspective. *Journal of Geodynamics*, **158**, 1-21. https://doi.org/10.1016/j.jog.2023.102005
[119] Scotese, C.R., 1991. Jurassic and Cretaceous plate tectonic reconstructions. *Palaeogeography, Palaeoclimatology, Palaeoecology*, **87**, 493-501. https://doi.org/10.1016/0031-0182(91)90145-H
[120] Stampfli, G.M. and Kozur, H.W., 2006. Europe from the Variscan to the Alpine cycles. *Geological Society, London, Memoirs*, **32**, 57-82. https://doi.org/10.1144/GSL.MEM.2006.032.01.04
[121] Arkell, W.J., 1956. *Jurassic Geology of the World*. Olivier and Boyd, London, 808 p.
[122] Makridin, V.P., Katz, Y.I., Kuzmicheva, E.I., 1968. Principles, methodology and significance of fauna of coral constructions for zoogeographic zonation of Jurassic and Cretaceous seas of Europe, Middle Asia, and adjacent countries. In: (Smirnov, G.A. and Kluzhina, M.L., Eds.), *Fossil Organogenic Constructions and Methods of Their Studying*. Ural Branch of the USSR Acad. of Sci., 184-195 (in Russian).
[123] Feldman, H.R., 1987. A new species of the Jurassic (Callovian) Brachiopod *Septirhynchia* from the Northern Sinai. *Journal of Paleontology*, **61**, No. 6, 1156-1172. https://doi.org/10.1017/S002233600002953X
[124] Hirsch, F., 1988. Jurassic biofacies versus sea level changes in the Middle eastern Levant (Ethiopian province). *Trans. of the 2nd Intern. Symp. of Jurassic Stratigraphy*, Lisbon, 963-981.
[125] Hirsch, F. and Picard, L., 1988. The Jurassic facies in the Levant. *Jour. of Petroleum Geology*, **11** No. 3, 277-308. https://doi.org/10.1111/j.1747-5457.1988.tb00819.x
[126] Cooper, G.A. 1989. Jurassic Brachiopods of Saudi Arabia. *Smithsonian Contributions to Paleobiology*, **65**, 213 p.
[127] Alizadeh, A.A., Guliyev, I.S., Kadirov, F.A. and Eppelbaum, L.V., 2016. *Geosciences in Azerbaijan*, Vol. **1**. Geology. Springer, Heidelberg, N.Y., 239 p.
[128] Eppelbaum, L.V. and Katz, Y.I., 2023. Where were the initial sources of the allochthonous oceanic crust of the southern Easternmost Mediterranean formed? *Trans. of the Intern. Conf. "Mediterranean Geosciences Union 2023"* (Springer). Istanbul, Turkey, 26-30 Nov., 2023, 1-6.
[129] George, R.P., Jr., 1978. Structural petrology of the Olympus ultramafic complex in the Troodos ophiolite, Cyprus. *Geol. Soc. Amer. Bull*., **89**, 845-865).https://doi.org/10.1130/0016-7606(1978)89<845:SPOTOU>2.0.CO;2
[130] Chan, G.H.-N., Malpas, J., Xenophontos, C. and Lo, C.-H., 2008. Magmatism associated with Gondwanian rifting and Neo-Tethyan oceanic basin development: Evidence from the Mamonia Complex, SW Cyprus. *Jour. of Geol. Soc.* (London, U.K.), **165**, 699-709. https://doi.org/10.1144/0016-76492007-050
[131] Aldanmaz, E., van Hinsbergen, D.J.J., Yıldız-Yüksekol, Ö., Schmidt, M.W., McPhee, P.J., Meisel, T., Güçtekin, A. and Mason, P.R.D., 2020. Effects of reactive dissolution of orthopyroxene in producing incompatible element depleted melts and refractory mantle residues during early fore-arc spreading: constraints from ophiolites in Eastern Mediterranean. *Lithos*, **360–361**, 105438, 1-14. https://doi.org/10.1016/j.lithos.2020.105438
[132] Chen, C., Su, B.-X., Wang, C.Y., Uysal, I. and Yao, Z.-S., 2021. Mantle melting models of the Kızıldağ ophiolite in SE Turkey: Two types of partial melting processes in the oceanic upper mantle of southern Neo-Tethys. *Lithos*, **398-399**, No. 106348, 1-17. https://doi.org/10.1016/j.lithos.2021.106348
[133] Rui, H.-C., Yang, J.-C., Lian, D.-Y., Wu, W.W. and Guo, G.-L., 2022. Deep origin of mantle peridotites from the Aladağ ophiolite, Turkey: Implication from trace element geochemistry of pyroxenes and mineralogy of ophiolitic diamonds. *Journal of Asian Earth Sciences*, **228**, No. 105153, 1-16. https://doi.org/10.1016/j.jseaes.2022.105153
[134] Sharkov, E.V. and Khanna, S., 1987. Evolution of the upper mantle material in regions of intraplate magmatism: Case study of western Syria. *Doklady Acad. Sci. SSSR*, **297**, 684-686.
[135] Esperanca, S. and Garfunkel, Z., 1986. Ultramafic xenoliths from the Mt. Carmel area (Karem Maharal volcano), Israel. *Lithos*, **19**, No. 1, 43–49. https://doi.org/10.1016/0024-4937(86)90014-9

[136] Dobrzhinetskaya, L., Mukhin, P., Wang, Q., Wirth, R., O'Bannon, E., Zhao, W., Eppelbaum, L. and Sokhonchuk, T., 2018. Moissanite (SiC) with metal-silicide and silicon inclusions from tuff of Israel: Raman spectroscopy and electron microscope studies. *Lithos*, **310-311**, 355-368. https://doi.org/10.1016/j.lithos.2017.04.001

[137] Griffin, W.L., Gain, S.E.M., Adams, D.T., Huang, J.-X., Saunders, M., Toledo, V., Pearson, N.J. and O'Reilly, S.Y., 2016. First terrestrial occurrence of tistarite (Ti_2O_3): Ultra-low oxygen fugacity in the upper mantle beneath Mount Carmel, Israel. *Geology*, **44**, 815-818. https://doi.org/10.1130/G37910.1

[138] Griffin, W.L., Gain, S.E.M., Huang, J.-X., Belousova, E.A., Toledo, V. and O'Reilly, S.Y., 2018. Permian to quaternary magmatism beneath the Mt Carmel area, Israel: Zircons from volcanic rocks and associated alluvial deposits. *Lithos*, **314-315**, 307-322. https://doi.org/10.1016/j.lithos.2018.06.007

[139] Lu, J.-G., Griffin, W.L., Huang, J.-X., Dai, H.-K., Castillo-Oliver, M., O'Reily, S.Y., 2022. Structure and composition of the lithosphere beneath Mount Carmel, North Israel. *Contrib. to Mineralogy and Petrology*, **177**, 29, 1-16. https://doi.org/10.1007/s00410-022-01897-7

[140] Ma, C., Cámara F., Bindi, L. and Griffin, W.L., 2024. Toledoite, TiFeSi, a New Mineral from Inclusions in Corundum Xenocrysts from Mount Carmel, Israel. *Crystals*, **14**, 96, 1-11, https://doi.org/10.3390/ cryst14010096

[141] Eppelbaum, L.V., Vaksman, V.L., Kouznetsov, S.V., Sazonova, L.M., Smirnov, S.A., Surkov, A.V., Bezlepkin, B., Katz, Y., Korotaeva, N.N. and Belovitskaya, G., 2006. Discovering of microdiamonds and minerals-satellites in Canyon Makhtesh Ramon (Negev desert, Israel). *Doklady Earth Sciences* (*Springer*), **407**, No. 2, 202-204. https://doi.org/10.1134/S1028334X06020097

[142] Eppelbaum, L.V. and Vaksman, V.L., 2017. Makhtesh Ramon Complex Deposit (Southern Israel) –A Window to the Upper Mantle. *Intern. Journal of Mining Sciences*, **3**, No. 1, 1-28. http://dx.doi.org/10.20431/2454-9460.0301001

[143] Barakat, A.A.S. and Kandil, M.R., 2019. Diamond in the newly discovered kimberlite and related rocks, Central Eastern Desert, Egypt. *Proceed. of the XXXVI Intern. Conf. "Magmatism of the Earth and Related Strategic Metal Deposits"*, St. Petersburg, Russia, 36–42.

[144] Eppelbaum, L.V., Katz, Y.I. and Ben-Avraham, Z., 2023. Geodynamic aspects of magnetic data analysis and tectonic-paleomagnetic mapping in the Easternmost Mediterranean: A review. *Applied Sciences*, ***Spec. Issue*** "Ground-Based Geomagnetic Observations: Techniques, Instruments and Scientific Outcomes", **13**, No. 18, 1-44. https://doi.org/ 10.3390/app131810541

[145] Hancilar et al. (2023). Kahramanmaraş - Gaziantep Türkiye M7.7 Earthquake, 6 February 2023. Strong Ground Motion and Building Damage Estimations. *Preliminary Report*. Dept. of Earthquake Engineering, Bogazici University, Turkey.

[146] Ben-Avraham, Z., 1992. Development of asymmetric basins along continental transform faults. *Tectonophysics*, **215**, 209-220. https://doi.org/10.1016/0040-1951(92)90082-H

[147] Smit, J., Brun, J.-P., Cloetingh, S. and Z. Ben-Avraham, 2010. The rift-like structure and asymmetry of the Dead Sea Fault. *Earth Planet. Sci. Lett*., **290**, 74-82. https://doi.org/10.1016/j.epsl.2009.11.060

[148] Garfunkel, Z. and Ben-Avraham, Z., 1996. The structure of the Dead Sea basin. *Tectonophysics*, **266**, 155-176. https://doi.org/10.1016/S0040-1951(96)00188-6

[149] Sharon, M., Sagy, A., Kurzon, I., Marco, S. and Rosensaft, M., 2020. Assessment of seismic sources and capable faults through hierarchic tectonic criteria: implications for seismic hazard in the Levant. *Nat. Hazards Earth Syst. Sci*., **20**, 125-148. https://doi.org/10.5194/nhess-20-125-2020

[150] Eppelbaum, L.V., Katz, Y.I. and Ben-Avraham, Z., 2022. Advanced combined geophysical-geological mapping of the Sea of Galilee and its vicinity, In: (A. di Mauro, A. Scozzari, S. Soldovieri, Eds.), *Instrumentation and Measurement Technologies for Water Cycle Management*, Springer, 553-579. https://doi.org/10.1007/978-3-031-08262-7_23

[151] Ron, H., Freund, R., Garfunkel, Z. and Nur, A., 1984. Block rotation by strike-slip faulting: structural and paleomagnetic evidence. *Jour. of Geophysical Research*, B **89**, 6256-6270. https://doi.org/10.1029/JB089IB07P06256

[152] Bosworth, W., 2024. Continental rift asymmetry and segmentation – contributions from the African plate. *Jour. of African Earth Sciences*, **210**, 105128, 1-15. https://doi.org/10.1016/j.jafrearsci.2023.105128

[153] Artemieva, I., Thybo, H. and Kaban, M.K., 2006. Deep Europe today: Geophysical synthesis of the upper mantle structure and lithospheric processes over 3.5 Ga. In: (D.G. Gee and R.A. Stephenson, Eds.), *European Lithosphere Dynamics*, Vol. 32 of *Geol. Soc. London., Mem.*, 11–41. https://doi.org/10.1144/GSL.MEM.2006.032.01.02

[154] Elgabry, M., Panza, G.F., Badawy, A.A. and Korrat, I.M., 2012. Imaging a relic of complex tectonics: the lithosphere-asthenosphere structure in the Eastern Mediterranean. *Terra Nova*, **25**, No. 2, 102-109. https://doi.org/10.1111/ter.12011

[155] Alekseenko, S.V., Kuibin, P.A. and Okulov, V.L., 2008. *Theory of Concentrated Vortices: An Introduction*. Springer. Berlin – Heidelberg – N.Y., 505 p.

[156] Tselentis, G.-A. and Drakopoulos, J., 1990. Stress Transfer and Nonlinear Stress Accumulation at the North Anatolian Fault, Turkey. *PAGEOPH*, **132**, No. 4, 699-710. https://doi.org/10.1007/BF00876814

[157] Neev, D. and Emery, K.O., 1995. *The Destruction of Sodom, Gomorrah, and Jericho: Geological, Climatological, and Archaeological Background*. Oxford University Press, N.Y., 175 p.

[158] Stein, R.S., Barka, A. and Dieterich, J.D., 1997. Progressive failure on the North Anatolian fault since 1939 by earthquake stress triggering. *Geoph. Jour. International*, **128**, 594-604. https://doi.org/10.1111/j.1365-246X.1997.tb05321.x

[159] Hubert-Ferrari, A., Armijo, R., King, G., Meyer, B. and Barka, A., 2002. Morphology, displacement, and slip rates along the North Anatolian Fault, Turkey. *Jour. of Geophysical Research*, 107, 1-33. https://doi.org/10.1029/2001JB000393

[160] Hubert-Ferrari, A., Barka, A., Jacques, E., Nalbant, S., Meyer, B., Armijo, R., Tapponnier, P. and King, G.C.P., 2000. Seismic hazard in the Sea of Marmarafollowing the Izmit earthquake. *Nature*, 404, 269–273. https://doi.org/10.1038/35005054

[161] Nalbant, S.; McCloskey, J., Steacy, S. and Barka, A.A., 2002. Stress accumulation and increased seismic risk in eastern Turkey. *Earth and Planet Sci. Lett*., 195, 291-298. https://doi.org/10.1016/S0012-821X(01)00592-1

[162] Vannucci, G., Pondrelli, S., Argnani, S., Morelli, A., Gasperini, P. and Boschi, E., 2004. An Atlas of Mediterranean seismicity. *Ann. Geophys*., 47 (Suppl. No. 1), 247–306. https://doi.org/10.4401/ag-3276

[163] Şengör, A.M.C., Tüysüz, O., İmren, C., Sakınç, M., Eyidoğan, H., Görür, N., Le Pichon, X. and Rangin, C., 2005. The North Anatolian Fault: A New Look. *Annu. Rev. Earth Planet. Sci*., 33, 37-112. https://doi.org/10.1146/annurev.earth.32.101802.120415

[164] Zare, M., Amini, H., Yazdi, P., Sesetyan, K., Demircioglu, M.B., Kalafat, D. and Erdik, M., Giardini, D., Khan, M.A. and Tsereteli, N., 2014. Recent developments of the Middle East catalog. *Jour. of Seismology*, 18, 749–772. https://doi.org/10.1007/s10950-014-9444-1

[165] Öztürk, S., 2018. Earthquake hazard potential in the Eastern Anatolian region of Turkey: seismotectonic b and Dc-values and precursory quiescence Z-value. *Front. Earth Sci.*, **12**(1), 215-236. https://doi.org/10.1007/s11707-017-0642-3

[166] KeAi, 2023. The magnitude of the 2023 Turkish earthquake matches the largest in the country's history, according to new study (11 April 2023). *Phys.org*. Retrieved 18 July 2023.

[167] Cetin, H., Güneyli, H. and Mayer, L., 2003. Paleoseismology of the Palu-Lake Hazar segment of the east Anatolian fault zone, Turkey. *Tectonophysics*, 374, 163-197. https://doi.org/10.1016/j.tecto.2003.08.003

[168] Armijo, R., Flerit, F., King, G. and Meyer, B., 2004. Linear elastic fracture mechanics explains the past and present evolution of the Aegean. *Earth and Plan. Sci. Lett*., 217, 85-95, https://doi.org/10.1016/S0012-821X (03)00590-9.

[169] Hubert-Ferrari, A., King, G., Manighetti, I., Armijo, R., Meyer, B. and Tapponnier, P., 2003. Long-term elasticity in the continental lithosphere; modelling the Aden Ridge propagation and the Anatolian extrusion process. *Geophysical Jour. International*, 153, 111-132. https://doi.org/10.1046/j.1365-246x.2003.01872.x

[170] Jiang, X., Song, X., Li, T. and Wu, K., 2023. Special focus/Rapid Communication Moment magnitudes of two large Turkish earthquakes on February 6, 2023, from long-period coda. *Earthquake Science, **36** (2),169–174.* https://doi.org/10.1016/j.eqs.2023.02.008.

[171] Baptie, B. and Segou, M., 2023. The Kahmaran Maras earthquake sequence, Turkey/Syria. British Geological Survey (14 Febr. 2023). Retrieved 21 December 2023.

[172] Çen, K.Ö., Bray, J.D., Frost, J.D., Hortacsu, A., Miranda, E., Moss, R.E.S. and Stewart, J.P., 2023. February 6, 2023 Türkiye Earthquakes: Report on Geoscience and Engineering Impacts. (GEER Association Report 082 ed., 6 May 2023). Earthquake Engin. Research Inst. https://doi.org/doi:10.18118/G6PM34. National Earthquake Information Center (6 February 2023). M 7.8 - Kahramanmaras Earthquake Sequence I. United States Geological Survey. Archived from the original on 6 February 2023. Retrieved 15 July 2023.

[173] National Earthquake Information Center. M 7.5 – Kahramanmaras Earthquake Sequence II. United States Geological Survey. Archived from the original on 6 February 2023. Retrieved 15 July 2023.

[174] Mikhailov, V.O., Babayantz, I.P., Volkova, M.S., Timoshkina, E.P., Smirnov, V.B. and Tikhotskiy, S.A., 2023. The February 6, 2023, Earthquakes in Turkey: A Model of the Rupture Surface Based on Satellite Radar Interferometry. *Doklady Earth Sciences* (Springer), **511**, 571-577. https://doi.org/10.1134/S1028334X23600627

[175] Gass, I.G., 1968. Is the Troodos Massif of Cyprus a fragment of Mesozoic ocean floor? *Nature*, **220** (5162), 39-42.

[176] Le Pichon, X., Chamot-Rooke, N., Lallemant, S., Noomen, R. and Veis, G., 1995. Geodetic determination of the kinematics of central Greece with respect to Europe: Implications for eastern Mediterranean tectonics. *Jour. of Geophysical Research*, **100**, B7, 12,675-12,990. https://doi.org/10.1029/95JB00317

[177] Faccenna, C., Bellier, O., Martinod, J., Piromallo, C. and Regard, V., 2006. Slab detachment beneath eastern Anatolia: A 10 possible cause for the formation of the North Anatolian fault. *Earth Planet. Sci. Lett*., **242**, 85-97. https://doi.org/10.1029/2002JB001757

[178] van Hinsbergen, D. J. J., Dekkers, M. J., Bozkurt, E. and Koopman, M., 2010. Exhumation with a twist: Paleomagnetic constraints on the evolution of the Menderes metamorphic core complex, western Turkey. *Tectonics*, **29**(3), TC3009, 1-33. https://doi.org/10.1029/2009TC002596

[179] Kaymakci, N., Langereis, C., Özkaptan, M., Özacar, A. A., Gülyüz, E., Uzel, B. and Sözbilir, H., 2018. Paleomagnetic evidence for upper plate response to a STEP fault, SW Anatolia. *Earth and Planetary Science Letters*, **498**, 101–115. https://doi.org/10.1016/j.epsl.2018.06.022

[180] Jolivet, R., Jara, J., Dalaison, M., Rouet-Leduc, B., Özdemir, A., Dogan, U., Çakir, Z., Ergintav, S. and Dubernet, P., 2023. Daily to Centennial Behavior of Aseismic Slip Along the Central Section of the North Anatolian Fault. *Jour. of Geophysical Research*: Solid Earth, **128**, e2022JB026018, 1-17. https://doi. org/10.1029/2022JB026018

[181] Orovetsky, Yu.P. and Kobolev, V.P., 2008. Connection of geostructures of the main surfaces of the Earth. Trans. of the 12th Intern. Conference "*Relationship Between the Surface and Deep Sstructures of the Earth's Crust*", Petrozavodsk, Russia, 99-102 (in Russian).

[182] Trubitsyn, V.P., 2010. The nature of the boundary between the upper and the lower mantle and its influence on convection. *Izvestiya, Phys. of the Solid Earth*, **46**, 461-476. https://doi.org/10.1134/S1069351310060017

[183] Kovachev, S.A. and Krylov, A.A., 2023. Microseismicity of the Persian Gulf and the Zagros Mountain Massif according to bottom seismological observations. *Volcanology and Seismology*, No. 6, 41-59. https://doi.org/10.31857/S0203030623700335

[184] Lusk, A.D., Chatzaras, V., Aldanmaz, E. and Tikoff, B., 2023. Hydration State and Rheologic Stratification of the Lithospheric Mantle Beneath the North Anatolian Fault, Turkey. *Geochemistry, Geophysics, Geosystems*, **24**, e2023GC011096, 1-26. https:// doi.org/10.1029/2023GC011096

[185] Taylor, R.N. and Nesbitt, R.W., 1988. Light rare-earth enrichment of supra subduction-zone mantle: Evidence from the Troodos ophiolite, Cyprus. *Geology*, **16**, 448-451. https://doi.org/10.1130/0091-7613(1988)016<0448:LREEOS>2.3.CO;2

[186] Eppelbaum, L.V. and Katz, Y.I., 2012a. Mineral deposits in Israel: A contemporary view, *In*: (Eds. Ya'ari, A. and Zahavi, E.D.) *Israel: Social, Economic and Political Developments*, Nova Science Publishers, N.Y., USA, 1-41.

[187] Skobelin, E.A., Sharapov, I.P. and Bugayov, A.F., 1990. Deliberations of state and ways of perestroika in geology (Has plate tectonics resulted in a revolution in geology?). In: *Critical Aspects of the Plate Tectonics Theory*. Theophrastus Publ., Athens, Greece, Vol. **1**, 17-37.

[188] Khain, V.E., 2001. *Tectonics of Continents and Oceans*. Nauchnyi Mir, Moscow, 606 p. (in Russian).

[189] Levin, B.F. and Chirkov, E.B., 1999. Features of the latitudinal distribution of seismicity and the rotation of the Earth. *Vulcanology and Seismology*, No. 6, 65–69 (in Russian).

[190] Eppelbaum, L.V. and Pilchin, A.N., 2005. Quick subsidence of a crustal block in SW Aegean Sea as a possible cause of the end of ancient civilization in the 17th century BC. *Trans. of the Intern. Conf. "Atlantis Hypothesis: Searching for a Lost Land"*, 11-13 July 2005, Milos Island, Greece.

[191] Ash, R.B., 2008. *Basic Probability Theory*. Dover Publications, Inc. Mineola, N. Y., 350 p.